

NASA Technical Memorandum 87184

Experimental Evidence for Modifying the Current Physical Model for Ice Accretion on Aircraft Surfaces

(NASA-TM-87184) EXPERIMENTAL EVIDENCE FOR
MODIFYING THE CURRENT PHYSICAL MODEL FOR ICE
ACCRETION ON AIRCRAFT SURFACES (NASA) 47 p
CSCL 01C

N88-12473

g3/03 Unclas
0111317

W. Olsen and E. Walker
Lewis Research Center
Cleveland, Ohio

Prepared for the
Third International Workshop on Atmospheric Icing of Structures
Vancouver, Canada, May 6-8, 1986

NASA

EXPERIMENTAL EVIDENCE FOR MODIFYING THE CURRENT PHYSICAL MODEL
FOR ICE ACCRETION ON AIRCRAFT SURFACES

W. Olsen and E. Walker
National Aeronautics and Space Administration
Lewis Research Center
Cleveland, Ohio 44135

SUMMARY

Closeup movies were taken of the icing process at several positions along the surface of a small airfoil for a range of airspeeds (50 to 320 km/hr), air temperatures (above freezing down to -25°C), and cloud conditions. These movies, still photographs (stop-action closeups), and other experimental data suggest that the current physical model for ice accretion needs significant modification at aircraft airspeeds.

At aircraft airspeeds there was no flow of liquid over the surface of the ice after a short initial flow, even at subfreezing temperatures that are close to the freezing point. Instead there were very large stationary drops on the ice surface that lose water from their bottoms by freezing and replenish their liquid by catching the microscopic cloud droplets. This observation disagrees with the existing physical model for aircraft icing, which assumes there is a thin liquid film continuously flowing over the ice surface. This constant flow was thought to be the main cause of horn-shaped clear (glaze) ice. With no significant water flow over the ice surface, the freezing-fraction concept of the current physical model fails when a mass balance is performed on the surface water. Rime ice forms when the air temperature is low enough to cause the cloud droplets to freeze almost immediately on impact; that aspect of the existing model is correct.

The movies and other results herein suggest the following changes to the current ice-accretion physical model. The characteristic shapes of horn-glaze ice or rime ice are primarily caused by the ice shape affecting the airflow locally and consequently the droplet catch and the resulting ice shape. In other words, ice that protrudes slightly will catch more droplets and, thereby, gradually grow faster than other nearby areas. Ice roughness plays a major role: it greatly increases the heat transfer coefficient, stops the movement of drops along the surface, and may also affect the airflow initially and, thereby, the droplet catch. At high subfreezing temperatures the initial flow and shedding of surface drops have a large effect on the ice shape; at the incipient freezing limit, no ice forms.

INTRODUCTION

The development and verification of analyses to predict the ice accretion on airfoils and other surfaces, and the resulting aerodynamic penalties are important parts of the NASA aircraft-icing research program. The purpose of the experimental study reported here is to determine if the existing physical model for ice accretion (refs. 1 to 3) is correct by obtaining direct photographic evidence. The current physical model is also the basis for the current icing scaling laws, which were recently described and evaluated in references 4 and 5.

Figure 1 shows how the ice shape changes when only the air temperature is changed. The fundamental question is, Why does the rime-ice shape form at -26°C and the horn-glaze shape form at -8°C ? The existing model gives the following physical reason for these different ice shapes. At the subfreezing air temperatures near the freezing temperatures, the microscopic cloud droplets impact the airfoil surface and form a thin film of water as shown in figure 2. A fraction of the incoming droplet-mass flux freezes where it impacts (the freezing fraction n of ref. 6); the remaining water in the thin film flows downwind along the ice surface. Much of this water film freezes downwind and creates the horn-shaped glaze ice. If all of the impacting droplets freeze on impact ($n = 1$), then rime ice forms. If $n = 0$ then no ice is formed. Reference 6 describes the icing process in this way, but details of the surface flow (such as whether there is a thin water film on the surface) are not described. The ice shapes predicted by these analytical models (refs. 1 to 3) have proven to be very sensitive to the air-side heat transfer coefficient used.

To investigate the basis of the existing physical model for the ice accretion process, detailed photographic data have been obtained in the NASA Icing Research Tunnel (IRT). This data consists of movies and stop-action still photographs of high enough magnification. The movies were made over a very large range of icing conditions, which include conditions that should favor a flow of water over the ice surface to form horn-shaped ice. Other types of data were also obtained to understand the ice accretion process better. These additional data pertain to the ice structure, surface roughness, the effect of the ice shape on droplet catch, and the effects of surface water flow and shedding. The movie supplement of this paper covers a far greater range of conditions than the previous movie on the subject (ref. 7).

NOMENCLATURE

| | |
|-----------|--|
| D | diameter of cylinder, μm |
| d | surface drop diameter, μm |
| H | height of surface drop, $H/d = 0.27$, μm |
| h | heat transfer coefficient of a dry airfoil or cylinder, usually at the stagnation point, $\text{cal}/\text{m}^2\text{-sec-}^{\circ}\text{C}$ |
| k | thermal conductivity of air, $\text{cal}/\text{m-sec-}^{\circ}\text{C}$ |
| L | characteristic size of surface for heat transfer, m |
| LWC | liquid water content of the icing cloud, g/m^3 |
| MVD | median volume diameter of the icing cloud, μm |
| \dot{m} | mass flux of impacting cloud droplets, $\text{g}/\text{m}^2\text{-sec}$ |
| n | conventional freezing fraction at stagnation line |
| Re | Reynolds number based on D |
| s | distance along airfoil surface from stagnation line, mm |

| | |
|-----------|--|
| t | static air temperature, °C |
| V | tunnel airspeed, km/hr |
| V_{top} | air velocity along top of surface droplets, m/sec |
| β | local droplet catch efficiency at stagnation point |
| δ | local average thickness of water layer or drops, μm |
| Δ | local average thickness of ice layer, μm |
| τ | time, sec |
| ρ_w | density of water, g/m^3 |
| ρ_s | density of ice, g/m^3 |

APPARATUS AND PROCEDURE

The movie and still photography setups, the Icing Research Tunnel (IRT), and sources of experiment error are described in this section. The test matrix and test procedures for each setup are also described.

Icing Research Tunnel

The IRT is a closed-loop refrigerated wind tunnel. Its test section (fig. 3) is 1.83 m high and 2.74 m wide. The airspeed in the test section can be varied from 30 to 480 km/hr. The total air temperature can be varied from about -1 °C down to at least -30 °C. Limited above-freezing data can also be achieved. The spray nozzles produce a drop-size range of 10 to 40 μm (median volume diameter, MVD). The liquid water content (LWC) in the center uniform region can be varied from about 0.3 to 3.0 g/m^3 . This range of LWC is not possible at every airspeed and MVD. For details about the spray-cloud calibration and a discussion of possible error sources in the icing simulation of the IRT refer to reference 8. The data reported here should be representative of a flight through natural icing conditions.

Movie Apparatus

The photographic setup to obtain closeup movies of the icing process along the airfoil surface is sketched in figure 4. The airfoil used in this study is sketched in figure 5. It is a symmetrical wooden airfoil of 11.4-cm chord and 12-cm span with a cylindrical leading edge of 1.9-cm radius. The airfoil is rigidly attached at each end of its 12-cm span by supports which are attached to the tunnel ceiling. The airfoil centerline is mounted 20 cm below the tunnel ceiling and at a 0° angle of attack with respect to the tunnel and the airflow. The movie camera, rigidly mounted above the tunnel ceiling, uses a high-magnification closeup lens arrangement. This lens views a small part of the airfoil surface through a view port in the IRT ceiling. A removable shield, located upstream of the airfoil, can be quickly removed to expose the airfoil to the droplet-laden airstream. Figure 6 is a photograph (looking

downstream) of the front part of the apparatus in the test section after a 5-min ice accumulation with the shield removed. The housing covering the telephoto lens can be seen (with ice on it) above the airfoil. The ice accretion on the airfoil leading edge is uniform which indicates that the LWC and velocity are uniform over much more of the airfoil span than photographed. The next question is, How much do the shield, airfoil end supports, and IRT boundary layer affect the local free-stream airspeed? The air velocity was measured at the location of the airfoil with the airfoil removed. The measured velocity agreed within 2 percent of the tunnel airspeed largely because the airfoil is well below the tunnel boundary layer (7 cm thick). The tunnel total temperature also agreed closely with the measured temperature at that location. After those checks the airspeed and total-temperature instruments of the IRT were used for these experiments. The droplet size of the icing clouds is uniform across the tunnel as shown by traverses with a laser spectrometer (ref. 8). The LWC, on the other hand, is not uniform across the test section. Measurements of the LWC at the airfoil location have shown that the LWC in that location is 30 percent of the LWC in the center of the IRT, where the IRT is calibrated. This local value of LWC is listed in table I.

The closeup movies were made using a 152-mm macrolens mounted on a 30-cm-long extension tube. The motion picture camera was a Fastex (model WF-3T). Sensitive color movie film (Kodak 7250 Tungsten) was used. All of the movies shown in the film supplement were taken at 24 frames per sec (real time) for the first 2 min after the dry airfoil was exposed to the icing cloud. Many movie sequences were also taken at 200 and 4000 frames per sec, and at higher magnification because it was initially thought that the fast-moving microscopic cloud droplets would impact and move across the surface before they froze. We only saw slow-moving very large drops on the surface, into which the microscopic cloud droplets impacted; therefore, no data from these early high-speed movies were used because they contain no additional information. The 24-frames-per-sec framing speed resulted in the following bonuses: greater depth of field and less heat from the lights.

The field of view (area of the airfoil that is photographed) is shown in figure 7. The horizontal lines painted on the surface of the airfoil are 0.3 mm (300 μm) thick and 2 mm (2000 μm) apart. The painted lines are covered with several layers of 3M Clear Protective Coating 3900, and each layer was sanded smooth so that the painted lines would not affect the ice accretion. The approximate location of the stagnation line is shown on the photograph. The airfoil angle varied slightly during the course of these experiments, which caused the stagnation line to move somewhat within zone 1. When the movie data are discussed we shall refer to different regions of the airfoil surface by the stagnation line and by zones 1, 2, and 3 which are shown in figure 5. For the later movies that show icing along the airfoil surface, reference dots were painted on the airfoil as shown in figure 5. The distance downstream of the stagnation line s is shown in figure 5 to correlate the various marks painted on the airfoil surface.

The rough surface on the right-hand side of the airfoil shown in figure 7 is the ice accretion for one 5-min-long icing condition; the ice on the left-hand side was melted with a warm aluminum block. Removing the ice in this manner permitted the ice shape to be accurately traced on a cardboard template that fit tightly on the upstream surface of the airfoil.

Two ELH photographic lamps illuminated the airfoil and the ice during the filming. Each had an air-cooled infrared filter to prevent any radiant heat from affecting the ice. The filters were quite effective as shown in reference 9. Comparison of the ice shapes accreted with and without the lights on showed that even the more intense lighting required for the 200-frames-per-sec films did not affect 5-min horn-glaze ice shapes.

Test Matrix and Procedure for the Movies

The test matrix is listed in table I. Data were taken over a range of temperatures, airspeeds, and drop sizes in the stagnation region of the airfoil. Data were also taken along the surface of the airfoil over a range of temperatures but for only one airspeed and drop size. Only the 24-frames-per-sec footage for the airfoil is listed.

The test procedure for most of the film sequences was as follows:

- (1) The airfoil was set at a 0° angle of attack. The camera was positioned to view the desired region of the airfoil surface.
- (2) The f-stop was adjusted to the light level, and the camera was focused on the dry airfoil surface.
- (3) The shield was moved down in front of the airfoil.
- (4) The wind tunnel airspeed, temperature, and spray conditions were set.
- (5) When the above conditions were steady the film was started, and the shield was quickly removed to start the film sequence with a dry airfoil. A few sequences start with rough ice; in those cases the camera was focused on the ice.
- (6) Each film sequence was 2 min long at 24 frames per sec.
- (7) The spray was often continued until 5 min of ice accreted on the airfoil surface so that the ice could be traced and photographed after it attained its distinctive shape.
- (8) The ice was melted off the airfoil and the apparatus, then the next test condition was run following steps 1 through 7.

Still Photography Apparatus and Procedure

The photographic setup for taking closeup still photos of the ice at a grazing angle is sketched in figure 8. The closeup still photos give clear black and white pictures of the icing process from a side-view perspective. Although very few icing conditions were photographed, most of the significant phenomenon observed in the movie film sequences are shown. Cross section AA on figure 8 shows the very small field of view which is centered on the stagnation line of a raised metal pad. A 135-mm macrolens with 43 cm of extension tubes was attached to an Olympus OM-2 single-lens reflex camera. An electronic flash was used to backlight the ice on the raised pad. The automatic flash mode of this camera, with its built-in lightmeter, was used to automatically

adjust the flash duration. The effective shutter speed measured was about 0.0001 sec, which would cause the fast-moving cloud droplets to appear as short streaks on the film. The same is true for any droplet moving along the surface because of bouncing or splashing. The motion of large surface drops would be stopped because they are much slower. The camera, flash, and raised pad were rigidly attached to a 2.5-cm-diameter pipe. This apparatus was rapidly inserted through a hole in the IRT ceiling and into the icing cloud; the raised pad was 0.63 m below the tunnel ceiling. Flash pictures were taken as rapidly as the flash would recharge in the automatic mode. When the ice grew too thick the apparatus was removed and cleaned for another run.

RESULTS AND DISCUSSION

The main purpose of collecting the photographic data in this experimental study was to determine if the existing physical model for ice accretion (refs. 1 to 3 and 6) is correct. In that physical model (fig. 2) the cloud droplets impact the surface and form a thin film of water, which flows along the surface and loses water by freezing. This surface flow has been used to explain the horn shape of clear (glaze) ice shown in figure 1. When the air temperature is very cold, the cloud droplets are thought to freeze on impact forming the rime ice shape shown in figure 1.

Most of the detailed data in this paper will come from the film supplement of this paper. However, we will describe the physics of icing that is seen in the film sequences by showing equivalent grazing-angle still photographs. The results from the film sequences will be plotted to show the quantitative effects of air temperature, airspeed, and cloud-droplet size. Analytical modelers of the icing process would find it helpful to borrow the film supplement for additional details. An abbreviated version of the film supplement that shows the essential physics is also available with narration (ref. 7). After describing the photographic data, other data that are helpful in determining a more correct physical model for icing are described. These data involve the ice structure, the effect of ice shape on the droplet catch, the effects of ice roughness, and the effect of surface flow and shedding. The consequences of the movie results on the mass and heat balance where freezing occurs are also discussed.

The icing conditions for the very detailed film supplement of this paper are listed in table I and are summarized as follows:

- Stagnation region, and also along the airfoil surface where cloud droplets impact
- High and low airspeeds: 320, 160, and 50 km/hr
- Total air temperatures above and below freezing:
5 °C; -1, -3, -7, -12, and -18 °C
- Cloud droplet sizes (MVD): 15 and 30 μm
- Moderately high LWC: 0.25 to 1.6 g/m³

Film sequences were not made of all of the possible combinations of variables listed. For example, photos of the icing along the airfoil surface (downstream direction) were only made at 320 km/hr and 30 μ m. Film sequences were made at the three airspeeds to satisfy the needs of aircraft and ground-structure icing. Most film sequences show the effect of air temperature in detail.

Photographic Results

We will start with the photographic data above freezing to show how the liquid flows when there surely will be a flow of liquid over the surface. Following that introduction, the photographic data for below freezing will be described.

Above freezing conditions. - The above-freezing results describe the flow on the surface that was caused by the impact of tiny cloud droplets, but without the major influence of freezing. In looking ahead, the main icing application for these above-freezing results is to partially describe the short initial time when there is water flow over the surface at below-freezing conditions. The total air temperature for these runs was above freezing, typically about 5 °C. At this temperature there certainly will be a flow of water over the surface of the airfoil. The above-freezing film sequences are 1 to 9 in table I.

Figure 9(a) is a closeup, grazing-angle still photo of what icing on the surface looks like a short time after the surface was exposed to the cloud. As stated previously, these closeup still photos of the surface of a cylinder show the same icing process as the movie results, but from a better angle and much more clearly when printed. The still camera is looking from a grazing angle along the stagnation line of the cylinder as shown in figure 8. The depth of field (i.e., nearest to the farthest distance in focus) in figure 9(a) is only a few thousand microns deep. The air and cloud droplets are coming in from the top of the picture. You can see the incoming microscopic cloud droplets as streaks (streaks retouched in a few figures to ensure visibility when printed). Hundreds of these microscopic cloud droplets impact the surface and form each of the large drops on the surface. These large surface drops will coalesce into progressively larger surface drops. The movie sequences show that when the surface drops grow large enough, the aerodynamic forces overcome the surface tension (adhesion) forces that are keeping the surface drops stationary, and the drops move downwind along the airfoil surface. Some drops that are moving to the right, away from the stagnation line, are shown in figure 9(b) by their trailing tail. As the large surface drops move along the surface, they sweep up other surface drops in their path and leave a relatively clear path behind them, where the surface drop growth process begins again from the impacts of cloud droplets. The growth and movement of the large surface drops become especially evident when the film sequences are played backwards.

The effect of airspeed on the surface drop size is shown by the photographs in figure 10. These individual frames from the movie were taken shortly before the first shed of surface drops in the stagnation region. At the lowest airspeed all of the very large drops shown in figure 10 coalesced into one gigantic drop and shed in the time of two additional movie frames. Two conclusions are immediately obvious: the surface drop size that shedding permits decreases with increased airspeed, and the drop size also decreases downstream of the stagnation region.

Figure 11(a) shows quantitative data from the film sequences above freezing. The size of the surface drops, just before they start to accelerate and rapidly move downwind, are shown as a function of the airspeed. This comparison was made at the same cloud-droplet size, $15\ \mu\text{m}$, and the same incoming cloud-droplet mass flux, ($\text{LWC}\cdot\text{V} = \text{constant}$). This quantitative data was measured from film sequences 1 to 4 and 7 to 9. Figure 11(a) also shows the surface-drop size just before the aerodynamic forces exceed the adhesion forces and the surface drops accelerate downwind. This acceleration of the surface drops is called shedding here even though the drops probably do not leave the surface completely, as evidenced by the fact that surface drops in the way downstream are cleared away. The size of the surface drops decreases inversely proportional to the square of the airspeed, which suggests a constant Weber number would correlate the data. Figure 11(a) also shows that the surface drops grow larger in the stagnation region before they move and shed. The time required to grow and coalesce to the drop size shown in figure 11(a) is plotted in figure 11(b) for $15\text{-}\mu\text{m}$ cloud droplets. Thirty-micron data agreed with the $15\text{-}\mu\text{m}$ data when the times were corrected to the same incoming droplet mass per unit area ($\text{LWC}\cdot\text{V}\cdot\text{time} = \text{constant}$).

Figure 12(a) is a plot of the steady-state drop diameter d along the airfoil surface. All measured surface-drop sizes in this paper are taken from an average of many drop measurements recorded in the film supplement. This figure shows that only small surface drops can survive aerodynamic shedding off the airfoil surface downstream of the stagnation region. This result is not surprising because the air velocity pushing and shedding the surface drops is much lower in the stagnation region. Surface tension and movement causes the height of the large surface drops to be about 27 percent of their diameter ($H/d = 0.27$, refs. 10 and 11). The surface drop height was calculated from the measured drop diameters in figure 12(a) and plotted in figure 12(b). The Weber number, which is the ratio of the aerodynamic forces moving a drop along the surface to the surface tension adhesion forces resisting the movement of the drop, can probably be used to understand why big surface drops shed, leaving only small drops moving along the surface downstream of the stagnation region. The velocity across the top of these surface drops V_{top} was approximately calculated from a Navier-Stokes aerodynamic computer code (ref. 12) for wholly turbulent flow over a smooth airfoil. It was found that $V_{\text{top}}^2 \cdot d$, the non-constant terms of the Weber number, was very low in the stagnation region ($s < 2\ \text{mm}$) and very large where the large surface drops were shedding (fig. 12(b)). This may explain why very large surface drops do not shed in the stagnation region but do shed immediately downstream where the boundary layer is much thinner. The viscous sublayer thickness was also estimated from the calculated velocity profiles. A short distance downstream of the stagnation point, the viscous sublayer thickness was very much thinner than the height of the surface drops. This means the flow over the drop-covered surface, which is the minimum (initial) roughness of a glaze ice surface, is aerodynamically fully rough. As you will see later, this has a large effect on the heat transfer coefficient downstream of the stagnation region.

None of the above-freezing film sequences showed any evidence of a flowing film of liquid. Instead, at all airspeeds the flow of liquid on the surface was entirely carried by the movement of very large surface drops, which shed off the surface wherever they got too big. Apparently, the minimum energy requirement when surface tension forces dominate (i.e., minimum surface area for a given mass) requires the largest possible drops. But as we will see later when we look at the below-freezing results, a water film is possible when

freezing removes enough water to prevent these large surface drops from forming.

The same above-freezing experiment was performed with a rough artificial ice surface (film sequence 5). Once again, all flow over the surface was carried by large surface drops. These surface drops grew larger before they moved because the rough surface of the artificial ice increased the adhesion forces as described in reference 10. All of the above-freezing results in the movie show that any significant surface water flow from impacting tiny cloud droplets will be carried over smooth or rough surfaces (e.g., ice) by large surface drops. This happens above freezing because surface tension dominates with small drops.

The tiny cloud droplets in the movie sequences cannot be seen because they are too small and fast moving. Nevertheless, you can see the result of their impacts into the large surface drops. The large surface drops shimmer when there is an impact (i.e., the reflection of the lights on the surface of the drops shimmer). When the spray cloud is turned off, the shimmering stops (film sequence 42). This shimmering is often interpreted incorrectly in ordinary ice accretion experiments as a surface flow of water. The closeup movies indicate that the initial surface flow actually stops when an observer several feet from the airfoil no longer sees the downstream edge of the ice moving downstream.

The effect of the airfoil material was determined by a simple experimental comparison. The shape of the large stationary surface drops did not change measurably when smooth aluminum or stainless steel were substituted for the plastic-coated airfoil of this experiment.

One rare event was observed in the dozens of grazing-angle photographs above freezing. Figure 13 shows the streaks of the reflections from splashed cloud droplets that were nearly stopped by the 0.0001-sec effective exposure time. In reference 13 it is noted that only big cloud droplets splash. In fact, the authors concluded that splash was so rare with the microscopic droplets of an icing cloud that it could probably be ignored. Therefore, the event seen in figure 13 was probably caused by a rare, big cloud droplet striking a large surface drop. Splashed or bouncing cloud droplets would be too small and fast moving to be seen in the movie sequences. The splashed and side-moving cloud droplets in the stop-action still photographs were counted and compared to the number of incoming cloud droplet streaks. This comparison suggests that no significant flow is carried over the surface by splashing or bouncing cloud droplets above freezing. There was no evidence of splashing or bouncing droplets in the below-freezing photographs in the stagnation region. Nevertheless, many more still photographs along the ice surface are needed to be statistically confident that splashed and bounced cloud droplets can be neglected at below-freezing conditions. Possibly, a better way to resolve the splashed droplet question may be to use a laser velocimeter to statistically measure the droplet size, velocity, and direction just above the ice surface with the icing cloud on.

With the above-freezing liquid flow model established, we can now move on to the below-freezing photographic data and see if there will be a flow of large drops over the ice surface as required by the existing ice accretion model.

Below-freezing conditions. - Before the below-freezing movie sequences and still photographs are discussed, it is helpful to look at the ice shapes that formed on the airfoil for the icing conditions of one set of movie sequences. The ice shapes that formed during a 5-min spray at the icing conditions of film sequences 10 to 14 are shown in figure 14. These shapes were obtained by tracing the ice after its edge was exposed by melting half the ice as shown in figure 7. The icing conditions for the ice shapes in figure 14 are airspeed, 320 km/hr; MVD, 30 μm ; LWC, 0.5 g/m³; white-rime ice shapes formed at the coldest temperatures (-18 and -23 °C). By merely increasing the air temperature to -3 °C the ice structure and shape changed to clear (glaze) ice with horns. The current physical model for icing (refs. 1 to 3) says that horn-glaze ice shapes are mainly caused by a steady flow of water over the ice surface, away from the stagnation region. In that model a fraction of the cloud droplets that impact in the stagnation region (the freezing fraction) freeze there; the remainder flows along the ice surface to the next incremental area downstream where the energy balance determines how much of the incoming water freezes, and so on downstream. Based on results seen in the above-freezing film sequences, the flow of liquid over the surface will probably be large drops. With rime ice there is no surface flow because the cloud droplets freeze essentially on impact.

The results from the below-freezing film sequences (10 to 42) are now discussed. As previously stated, we shall primarily use the more descriptive grazing-angle still photos to show the icing process seen in the movies, because the physical model shown by both is the same.

The horn-glaze and rime ice shapes at -3 and -18 °C in figure 14 were obtained after a 5-min exposure in the icing conditions of film sequences 11 and 14, respectively. All physical changes seen in film sequence 11 are the same as those seen in the still photo sequence shown in figures 9 and 15. Sequence 11 is for an airspeed of 320 km/hr, a total air temperature of -3 °C, and a cloud-droplet size of 30 μm . Even though the photographs in figures 9(a) and (b) were taken above freezing, they also show the events seen in the first few seconds of film sequence 11. The initially dry airfoil surface is quickly covered by large rapidly growing drops as shown in figure 9(a). Soon some of the larger surface drops begin to move away from the stagnation line as shown by figure 9(b). After a few seconds all surface drops stop moving in the stagnation region because the adhesion forces greatly increase on a rough surface (ref. 10) such as glaze ice. The highly coupled effects of surface tension and freezing (roughness and energy balance) then result in the following changes in the surface. After about 30 sec of icing, the ice surface looks like figure 15(a). In the stagnation region, freezing causes the initial big surface drops to be replaced by a thin film of water with a thin ice layer and ice hills (about 1000 μm across) growing underneath. Outside the thin-film region very large stationary ice hills are forming. The hills near the thin-film region have smooth tops because they are covered with large water drops, which shimmer when cloud droplets impact the surface. The photographs in figures 15(b) and (c) show what film sequence 11 shows at about 55 and 75 sec, respectively. You can see that the thin-film region has been gradually replaced by large stationary ice hills that are about 1000 μm in diameter. The ice hills that are far from the thin-film region have a rough surface, which indicates those ice hills are not covered with water.

Figures 16(a) to (c) are black and white prints of three individual frames from movie film sequence 11. Black and white stills from a color movie simply do not show the icing process nearly as well as the original movie.

A grazing-angle view of the rime-ice surface at $-18\text{ }^{\circ}\text{C}$ (film sequence 14) is shown in figure 17. Rime ice is clearly a much smoother surface than glaze (clear) ice where cloud droplets impact.

The physical attributes that can be measured from the movie are visual effects: the size and movement of the surface drops, and the presence of thin-water film, glaze ice, or rime ice. These physical attributes of the icing process change with airspeed, time, and temperature, etc. We shall use the detailed movie results to quantitatively describe how those physical attributes change.

The time when the initial flow of surface drops stop moving because of freezing is easily obtained from film sequences 10 to 14. The drop-stopping time along the airfoil surface is plotted in figure 18 for a range of air temperatures at an airspeed of 320 km/hr. The time duration of surface flow increases as the air temperature and distance along the airfoil are increased. It is believed that the main reason the surface drops stop moving is because freezing creates some rough ice which greatly increases the surface-tension adhesion forces (ref. 10) and prevents the aerodynamic forces from moving the drop. The main point of figure 18 is that there is no flow of water over the surface after a very short time, 1 sec in the stagnation region. This time is especially short when compared to the time of a typical exposure in natural icing. In fact all surface water flow stops after about 1 min for the warmest total air temperature run, $-1.1\text{ }^{\circ}\text{C}$.

The conventional freezing fraction in the stagnation region, which is essentially constant with time (refs. 1, 2, and 6), was calculated for the warmest case in figure 18 to be about 0.2. This means that the water flow leaving the stagnation region on the ice surface would be about 80 percent of the surface flow seen in the above-freezing movies (see film sequence 1). As figure 18 shows, there is no surface flow in the stagnation region for this case. We shall discuss this in more detail later and show that the conventional freezing-fraction concept used in current ice accretion theory is physically incorrect.

In addition to the initial movement of surface drops, there is another growth history occurring where a thin film of water and ice grow. This is gradually replaced by the growth of large stationary surface droplets on top of ice hills (fig. 15). Figure 19 shows quantitative data for the growth history of these large surface drops in the stagnation region (zone 1) over a range of air temperatures. The impacting mass flux of microscopic cloud droplets is the same for all cases in figure 19, but the mass flux removed from the water by freezing increases with reduced air temperature. Compare the surface-drop growth in zone 1 (stagnation line) at $-1.1\text{ }^{\circ}\text{C}$ with the growth at $-12\text{ }^{\circ}\text{C}$. The formation of large surface drops is delayed at $-12\text{ }^{\circ}\text{C}$ because the freezing rate is large enough to slow down the growth of the water-layer thickness in the thin-film region (see fig. 15). Figure 19 shows that these large stationary surface drops grow rapidly, once they start to form, and then much more slowly because the drops get packed together, and the large surface drops on

the ice hills do not coalesce too often. A similar growth history occurs downstream, but the surface drops there start growing sooner than in the stagnation region.

Figure 20 shows how the "large-time" drop size on top of the ice hills changes downstream along the surface of the ice. These diameters were measured at 80 sec, when the growth rate is much slower, as shown in figure 19; it is also near the end of the available film footage for each sequence. Figure 20 shows that the large-time average-drop diameter increases slowly downstream along the ice surface. The above-freezing surface-drop diameter from figure 12 is also plotted in figure 20 to show the effects of freezing on the drop size along the airfoil surface. The difference is that for above-freezing conditions, shedding prevents big drops from forming downstream, whereas the increased adhesion of the rough ice greatly reduces shedding.

Table II shows how the physical attributes of the ice change with airspeed and temperature. (See table footnotes for a description of the ice formed.) Velocity has a profound effect on the appearance of the ice. At the highest airspeed run (320 km/hr), which is on the low end of aircraft speeds, the initial surface flow of large drops stops in less than a second in the stagnation region. At the lowest airspeed run (50 km/hr), there is flow over the surface for at least the whole 2-min-long film sequence. The description of surface flow at 160 km/hr is between the descriptions for the high and low airspeeds. There is clear evidence of a slow flow in the thin-film region at -7 and -12 °C for 160 km/hr. No such flow was observed in the thin-film region at 320 km/hr, probably because the water film was too thin. The current physical model for icing (i.e., current understanding of icing physics in refs. 1 and 6) was apparently based on experimental macroscopic observations at low airspeeds.

Other Supporting Data

This section includes a variety of other data that will be very helpful in formulating a more correct physical model for icing. These additional data pertain to the ice structure, the effect of the ice roughness and shape on the cloud droplet catch, and the effects of the initial liquid flow and shedding. Also included are the consequences of what was observed photographically on the mass and heat balances where freezing occurs. Then finally all of the key results are put together to describe modifications to the current model that should result in a more correct physical model for ice accretion.

Evaluation of the freezing-fraction concept. - The existing physical model of icing (refs. 1, 2, and 6) states that horn-glaze ice shapes form because there is a flow of liquid over the ice surface. The biggest horns occur at high airspeeds (ref. 14). The closeup movies at a high airspeed (e.g., sequences 10 to 19) showed that there is no surface flow of water after a short initial flow. Let us now do a conventional mass balance on a unit area where freezing occurs in the stagnation region.

$$\dot{m} = \beta \cdot \text{LWC} \cdot V = \rho_l \frac{\partial \delta}{\partial t} + \rho_s \frac{\partial \Delta}{\partial t} - \text{Net water flowing out of unit area} - \text{Evaporation} \quad (1)$$

Impacting droplet mass flux Growth of water Growth of ice layer 0 after very short initial flow Negligible

The freezing fraction n in the stagnation region is conventionally defined (refs. 1, 2, and 6) as the fraction of the impacting-droplet mass flux \dot{m} that freezes in that unit area.

$$n\dot{m} = \rho_s \frac{\partial \Delta}{\partial t} \quad (2)$$

Substitute equation (2) into equation (1) and solve for the water-layer growth rate.

$$\frac{\partial \delta}{\partial t} = \frac{1}{\rho_l} (1 - n)\dot{m} \quad (3)$$

The freezing fraction for the stagnation region was calculated for film sequences 10 to 14 from the conventional energy balance (refs. 1, 2, or 6), which is independent of time. The heat transfer coefficient h used is the one used for the stagnation region of a dry airfoil or cylinder, where h is proportional to $(V/L)^{0.5}$. The calculated freezing fractions for all film sequences are listed in table I. The freezing fraction n is 0.28 for the horn-glaze ice shape in figure 14 (i.e., the -3°C shape, sequence 11). Substituting $n = 0.28$ into equations (2) and (3) shows that the water layer δ , must be about three times thicker than the ice layer Δ because there is no surface flow of water in the stagnation region after about 1 sec of initial flow (see fig. 18). The equation for h suggests that this initial flow will last perhaps two to three times longer for a full-sized airfoil, but that is not nearly enough to change the no-surface flow conclusion at aircraft airspeeds. The water layer of large drops or thin film seen in the movie sequences or still photos is much thinner than the ice layer, which totally disagrees with the result from the mass balance using the conventional freezing-fraction concept. In other words, the conventional freezing-fraction concept defined by the energy balance in reference 6 fails at aircraft airspeeds to correctly describe an essential aspect of the physics of icing, namely, the mass balance. We shall discuss a physically more correct replacement for the freezing fraction later. Table II shows that at low airspeeds the conventional freezing-fraction concept may be a good approximation because there clearly is a flow of liquid over the surface for a long period of time.

Other physical models that could also lead to the freezing-fraction concept must also be checked out experimentally. They are splashed or bouncing cloud droplets, and ice that is only partially frozen (i.e., slush). A splashed cloud droplet is evident in the photo of figure 13. As said previously, the fraction of splashed streaks to the incoming cloud-droplet streaks that were caught by the stop-action photos was so low that it could probably be ignored, especially over ice. Bounced cloud droplets were even rarer. The question of slush was checked out manually while glaze ice was growing in an icing cloud at an airspeed of 200 km/hr. By probing the ice surface with a needle on the end of a 2-ft-long hand-held rod, it proved easy to determine

that the ice was hard (not slush); it was also easy to feel that the ice was rough and to see that the water layer was very thin.

With surface flow removed as the major cause, another physical explanation is required to explain horn-glaze ice shapes at aircraft airspeeds. We shall describe what we hope is a more accurate physical model for icing by introducing additional data which supports and expands on the photographic data already introduced.

Ice structure. - Three figures were selected from the data in reference 14 to describe the ice structure. These figures will be described, and then their illustration of the icing process will be discussed.

Figure 21 contains tracings of the ice shapes and photographs of three kinds of ice on the pressure side of an airfoil at a low aircraft airspeed. The horn-glaze ice on figure 21(a) is clear everywhere (like an ice cube) and has a rough surface everywhere. The ice on figure 21(c) is entirely composed of rime ice, which is white and opaque everywhere. Rime ice is smooth on the upstream surface, where cloud droplets impact and as rough as glaze ice on the sides. Figure 21(b) is mixed ice, which our extensive ice structure data shows to be always made up of distinct glaze and rime ice parts: in the stagnation region it is clear ice, and rime ice forms downstream of the clear ice. The fraction of the total ice accretion that is made up of rime ice depends upon the local energy balance. Downstream of the ice cap, ice fingers form that are either glaze (clear) or rime ice.

Let us now look at the structure of the ice cap in detail. To do that the ice cap was removed from the airfoil and thin ice samples (0.3 cm thick) were sliced off with a very small steam knife (ref. 14). These ice samples were then backlighted and photographed. Figure 22 shows these backlighted ice samples that were accreted at the same icing conditions with only the air temperature changed. The icing conditions at -8, -15, and -26 °C are exactly the same as those for figure 21. When white rime ice is backlighted it appears black because it is opaque. The ice at -2 and -8 °C is entirely clear (glaze) and has large air bubbles throughout. The clear ice region of the ice formed at -15 and -18 °C is filled with curious streaks, which on close inspection are actually continuous curved wire-like filaments. These observations will be discussed in more detail shortly.

About 60 ice structure measurements have been made over a large range of icing conditions for one airfoil. The gradual changes in the ice structure seen in figure 22 are representative of ice structure changes seen for the additional 60 measurements. All ice structure data are well correlated by the conventional freezing fraction calculated for the stagnation line of a dry airfoil. This suggests the nondimensional freezing fraction evaluated at the stagnation point of the dry smooth surface may be useful if it is thought of as a "freezing potential." The only negative vote was some large cylinder data with rime ice which did not correlate adequately.

Some clear (glaze) ice and rime ice samples were mechanically shaved so that they were very thin in order to show the crystal size in color with polarized light. Figure 23 is a black and white print of a typical glaze-ice sample and a rime-ice sample. Some ice was lost in making these very thin samples. Clearly, the crystal size for the glaze-ice samples is very large, and the crystals are oriented very much like the streaks for the ice sample at -15 °C

on figure 22. The rime-ice sample is clearly made up of much smaller crystals in the stagnation region. The ice-shaving process was not refined enough to prevent the formation of some large crystals by melting and refreezing.

Let us now discuss figures 21, 22, and 23 with respect to the observations made in the film supplement and still photographs. The existing physical model for icing shows that rime ice forms because the impacting cloud droplets freeze on impact, and air is trapped between the rapidly frozen droplets. That description appears to be essentially supported by figures 22 and 23. The crystal size in figure 23 is certainly very small, albeit much larger than single cloud droplets frozen on impact. Figure 22 shows that rime ice is opaque, which suggests that either air or frost from the vapor is trapped as the rime ice is accreted.

The movie sequences and the still photographs show that clear (glaze) ice is formed anywhere there is a large enough body of water on top of the ice, either as a thin film or as large surface drops. It appears that if the freezing rate is very close to the impacting cloud-droplet mass flux then there will not be a large enough covering layer of water to form clear (glaze) ice; therefore, rime ice will form there. This suggests that the type of ice formed at any location (rime or glaze) depends upon the local energy balance where freezing occurs. The consequence of this observation is discussed when the energy balance is discussed further. The large voids or bubbles in the glaze ice at -2 and -8 °C are discussed when the effect of the ice shape on droplet catch (fig. 24) is covered.

The streaks in the ice at -15 and -18 °C of figure 22 are a curious phenomenon that can be explained satisfactorily by the photographic data. The closeup movies at those conditions show large stationary surface drops that are closely packed in a fairly well-ordered array of nearly the same size drops. The grazing-angle still photographs in figure 15 show that large drops are on top of tall ice hills. These drops and hills grow outward as cloud droplets impact and freezing occurs on the ice hill. The deep cavities where three large surface drops and hills come together in this regular array of drops are believed to be the cause of the wire-like filaments (i.e., the streaks in figure 22). These wire-like filaments are believed to be rime ice, which is formed there because surface tension keeps the water out of those deep cavities; and the deep cavities prevent the impacts of cloud droplets. At higher temperatures (e.g., the -2 or -8 °C shapes on fig. 22) the distinct cavities between three surface drops do not stay in the same place for very long because of slow drop coalescing; therefore, no long streaks form. Some of the figures shown in the next section will add further information about the ice structure. The dozens of ice structure photos with these streaks showed that the local ice growth vector was along these streaks.

Effect of ice shape on cloud droplet catch. - The largest horns on glaze ice seem to occur at high airspeeds. The closeup movies showed that the existing physical model for ice accretion was incorrect; horns are not primarily formed by a continual flow of water over the ice surface. How then does a horn-glaze ice shape form at subfreezing air temperatures near freezing, and a rime-ice shape at low temperatures? A strong clue is given by figure 24 which shows the growth of horn-glaze ice and rime ice on a cylinder by means of dye growth rings. Every few minutes the cloud spray was stopped and the entire ice surface was sprayed with water soluble blue dye. After about 16 min of total spray time, the ice was removed from the stainless steel cylinder by

heat, and a thin sample of ice was photographed. (Other experiments showed that the ice shape resulting from several short sprays was the same as the shape from one long spray of the same total spray time and icing conditions.) The dye growth rings were traced from the photograph to show the rings more clearly. These dye growth rings show the following. First, there was no ice growth on the sides of the rime or glaze ice shapes. All of the ice growth occurred on the upstream face of the ice between points A-A. The maximum growth rate occurred along line B, which is the stagnation line for the rime ice and at the horns for the horn-glaze ice shape. The most important observation is that the final rime and horn-glaze ice shapes were obtained gradually. You can see that the characteristic horn and pointed rime shapes become gradually more pronounced as time increased. This gradual change in shape suggests that the ice shape gradually affects the local airflow and, therefore, the local droplet catch and resulting ice shape in an interactive bootstrap manner. In other words, the major reason for these two vastly different ice shapes is that ice that sticks out slightly will grow faster than its neighbors because it will catch slightly more cloud droplets.

The above contention was investigated by spraying a 3-min rime-ice condition on top of a horn-glaze ice shape and also on top of a rime-ice shape. The result of this experiment is shown by the photographs in figure 25. With rime ice, cloud droplets freeze essentially on impact. Therefore, the thickness of this 3-min rime-ice addition would be proportional to the local droplet-collection efficiency. Once again, we see that the ice accretion is only on the upstream faces of the ice. By measuring the thickness of the added rime ice it is easy to see that the droplet catch is greatest in the region of the horns for the horn-glaze ice shape. For the rime-ice shape, the thickness of the added rime ice shows that cloud droplet catch is greatest at the stagnation point. (Dye was used to separate the original rime ice from the added rime ice.) Figure 25 clearly shows that the ice shape has a strong effect on the local cloud-droplet catch and, therefore, on the ice shape that is accreted.

Of course, the different shapes for rime and horn-glaze ice are not completely caused by the effect of the ice shape on the droplet catch. The ice shape is certainly affected by any initial flow over the surface, and the effect of shedding of surface water drops is also important. The ice roughness, which is much larger for glaze ice than it is for rime ice, may affect the local airflow and droplet catch during at least the initial accretion of the ice. Indeed, the initial ice shape and roughness of rime and glaze ice may be different enough to start off the gradual bootstrap growth process that will eventually result in the characteristic ice shapes for rime and glaze ice.

Figure 25 also adds additional information about the ice structure. There are large voids throughout the original clear (glaze) ice, which are also apparent in figure 23. Notice that the large cavity in the surface of the glaze ice shape in figure 25 was not filled in by the added rime spray. The large voids in the glaze ice are clearly caused by the fact that the droplet-laden airstream will avoid a depression such as a cavity. The depression often seen along the stagnation line will get deeper in time as droplets avoid that area. Details of the rime ice structure are clearly shown in figure 25 by the dye. The thin backlighted rime ice sample shows that rime ice is made up of closely spaced fingers that grow "up-trajectory" and are tightly or loosely sintered together. The ice fingers downstream of the ice cap that are shown on figure 21 are well-separated fingers of ice. The size and number of these fingers do not seem to depend strongly on whether they are rime or glaze ice.

Ice roughness. - Ice roughness hills can be expected to grow larger with the passage of time because a hill will catch more cloud droplets. The effect of time on the surface roughness is shown by figure 26 from reference 14. The effect of temperature on roughness is shown in figure 27 from reference 14. Glaze ice is always much rougher than rime ice where droplets impact and freezing occurs. This is also shown by the closeup grazing-angle photos (figs. 15 and 17). The much greater roughness of glaze ice, compared to rime ice, will thicken the boundary layer of the air flow downstream of the stagnation line. This will deflect the airstream locally and cause droplets to be deflected more downstream initially than they would be with smooth rime ice. The local heat transfer coefficient will also be much higher for rough glaze ice than for smooth rime ice as shown below. Current ice accretion computer codes (e.g., ref. 3) use the effect of roughness on the heat transfer coefficient h . The roughness was initially empirically adjusted in order to calculate adequately correct ice shapes. It is disturbing to note that the roughness used to obtain glaze ice and rime ice shapes is opposite the roughness for glaze and rime ice observed experimentally. Specifically, smooth ice (i.e., low h) is required to produce glaze ice shapes, but figure 27 shows that glaze ice (colder than -12°C) is much rougher than rime ice (-26°C).

Local heat transfer coefficient. - The local heat transfer coefficient was measured along the surface of plastic horn-glaze and rime-ice shapes with local heat meters (ref. 15). Plastic horn-glaze ice shapes were made of the 2-, 5-, and 15-min ice accretions that formed on a 5.2-cm cylinder at the same icing conditions. These ice shapes are shown in figure 28 along with the 15-min rime-ice shape. Smooth and rough surfaces were tested in a wind tunnel airstream whose turbulence intensity was 0.5 percent (typical of the IRT). Heat transfer data were taken over a range of airspeeds so that the local variation of the heat transfer correlation terms (A and B) could be determined along the surface of the simulated ice shapes and the cylinder.

$$\frac{hD}{k} = A \text{Re}^B \quad (4)$$

This data was used to estimate how h , A, and B vary with time along some obvious ice-growth lines. From the previous discussion about the ice roughness and the movie results, the ice growth history of 15-min horn-glaze ice shape would start with the smooth cylinder (i.e., initially dry cylinder) followed immediately by the rough cylinder (i.e., initial water drops and ice) as shown along the time scale of figure 28. These would then be followed by the 2-, 5-, and 15-min rough horn-glaze shapes. The rime ice-growth history would go from the initially dry (smooth) cylinder to the 15-min smooth rime-ice shape; rime ice is smooth where cloud droplets impact and freeze.

The values of h , A, and B at the stagnation line (growth line 0) for the glaze and rime ice shapes are plotted in figure 28 as a function of time. The values of h , A, and B at the stagnation line for the glaze and rime-ice shapes remain essentially the same as for a smooth dry cylinder at the stagnation line. Notice in particular that the Reynolds number exponent B stays at essentially 0.5. Most ice accretion theories (refs. 1 to 3) take advantage of this tremendous simplification. Unfortunately the values of h , A, and B change drastically a short distance downstream of the stagnation line. The values of h , A, and B along growth lines 1 and 2 for glaze ice are very different from their values along the stagnation growth line. The surface roughness of glaze ice causes h along growth lines 1 and 2 to quickly become two

to three times larger than the h at the stagnation line. The Reynolds number exponent B quickly becomes more nearly 0.8, the turbulent flow value. In other words the heat transfer from most of the glaze-ice surface (where droplets impact) to the cold air is much larger than the h most theories assume (i.e., the stagnation line h). When this much larger h value is used in the Messinger energy balance (ref. 6) the freezing fraction is greatly increased. If you also include the increased surface area of the large drops on the surface of glaze ice, the freezing fraction would exceed one so that there would be no surface flow to cause the horns. Even so there can still be a flow of surface water at higher temperatures and during the initial transient when the ice roughness rapidly increases; these are now discussed.

Effect of the initial surface flow. - The initial flow of surface drops moves water downstream; some of these moving drops shed which also affects the ice shape formed. These initial flow effects can give a start to a horn ice shape, as shown by the ice shapes in figure 29. The horn-glaze and rime ice shapes shown were accreted during 2-, 5-, and 15-min-long sprays on an airfoil at several angles of attack (0, 4, and 8°). By comparing the 2-min horn-glaze ice shapes at the different angles you can see the effect of the initial flow, especially at 8°. The initial flow should last somewhat longer for this larger airfoil than that seen in the closeup movies. The initial flow time in the stagnation region will still be nearly zero as shown by figure 18. The effect of the initial flow is also apparent in the 2-min glaze-ice growth ring in figure 24(a).

Ice growth directions were drawn as light dashed lines on the ice shapes shown in figure 29. As in figures 24 and 28, these lines simply connect obviously similar features of the ice shape (e.g., the horn, bumps, or dips). The ice growth along all the growth lines increases linearly with time, with the growth rate varying from line to line.

An interesting side issue comes from a comparison of the 2-min rime and glaze ice shapes for the 0 and 4° angles of attack. Even though the icing conditions are vastly different, the 2-min ice shapes are nearly the same, about as close as ice shape repeatability permits. This insensitivity suggests that one should not attempt to prove a theory works by making experimental comparisons of ice shapes with a small amount of ice. To avoid the ice shape measurement problem, aeropenalty measurements should always be made in any comparisons with a small amount of ice.

Effect of shedding. - The closeup movies for above-freezing conditions showed that the surface drops grew until they were large enough to move. Movement occurred when the aerodynamic forces acting on the drop exceeded the surface tension (adhesion) forces that prevent movement. As shown by figure 12, the surface drops downstream of the stagnation region are much smaller because the largest drops have shed off the surface there. Figure 30 shows that surface-drop shedding has a profound effect on the ice shape at the warmer sub-freezing temperatures even for a low airspeed of 209 km/hr. This conclusion is demonstrated by the rapid decrease in the cross-sectional area of the ice shape above about -5 °C. At -5 °C the conventional freezing fraction (stagnation line of a cylinder) at the stagnation line is 0.21 for the conditions in figure 30. There is obviously significant shedding of surface drops at -2 and -1 °C in figure 30, where the conventional freezing fraction is 0.11 and 0.08, respectively. Very little shedding is evident in the movie sequences at these temperatures because very few sequences have freezing fractions below 0.2. The

short initial flow transient will obviously be much longer for freezing fractions lower than 0.2. At much higher airspeeds (or rotation-caused G forces), ice will also shed.

The initial surface-drop growth, and the movement and shedding of surface drops must obviously be understood quantitatively before a correct ice accretion analysis can be formulated. The surface-drop data that can be obtained from the film supplement will prove quite useful in formulating an improved analysis involving momentum, mass, and energy balances for the surface water during the initial transient when there is a surface flow. When freezing starts the surface gets rougher and the increased adhesion stops the movement of the surface drops.

Suggested Changes to the Physical Model for Icing

For above-freezing air temperatures, large surface drops are formed from the microscopic cloud droplets impacting the surface of the airfoil, as shown in figure 31(a). When these drops are large enough for the aerodynamic forces to exceed the surface-tension-adhesion forces the surface drops start to move downstream. At low airspeeds these surface drops get very large before they move. As they move downstream the largest surface drops shed and leave only smaller drops on the surface downstream.

For below-freezing temperatures and aircraft airspeeds, these surface drops move over the surface for only a short time before the high surface-tension-adhesion forces of the rough ice that is beginning to form stops their movement. The surface-drop running time will be longer at the higher subfreezing temperatures. The running time is also longer for large airfoils or lower airspeeds because the heat transfer coefficient and, therefore, the freezing rate is lower. The physical model for icing observed in the movies and still photos is sketched in figure 31(b) and described in table II. At glaze-icing conditions, the stagnation region initially will have a thin water film region. As you move away from the stagnation line, the thin water film rapidly becomes replaced by very large stationary drops on top of ice hills. The width of the thin-film region decreases with time, and increases somewhat with decreasing temperature. Clear (glaze) ice is formed anywhere there is a liquid cover (big drops or a thin water film) over the ice. As the air temperature decreases, the freezing rate approaches the mass flux of the impacting cloud droplets. When this happens, a thin film of water cannot be maintained, and droplets freeze essentially on impact and form rime ice. The effects of varied icing conditions upon the physical model just described are listed in table III.

The thickness of the surface drops and/or the thin water film increases by the impact of cloud droplets while they lose water by freezing. The heat of freezing is transferred to the cold air through the slightly subcooled water on the surface of the ice.

Because there is no surface flow of water after a very short time, the conventional freezing-fraction concept fails when it is used in a mass balance where freezing occurs. The energy balance where freezing occurs also needs major changes to account for the following transient effects: the very large effect of roughness on the controlling air-side heat transfer coefficient and surface area for glaze ice, and the initial flow and shedding of the surface drops at high subfreezing temperatures. The greatly increased heat transfer

for rough horn-shaped glaze ice is sufficient to freeze nearly all of the impacting glazed droplets.

The ice shape that is formed initially is affected by the initial flow and shedding. The initial roughness and ice shape also affect the local airflow which, in turn, affects the local droplet catch so that the ice shape is slowly changed. Simply stated, ice that protrudes will accrete ice faster and depressions will get deeper. This gradual interactive bootstrap process is described step by step in figure 32 for horn-glaze and rime ice shapes. Unfortunately, bootstrap processes and processes that depend strongly on roughness are notoriously difficult to predict with any accuracy.

FUTURE PHOTOGRAPHIC WORK

Closeup grazing-angle movie data are required in the IRT with a larger airfoil in order to obtain data at freezing fractions lower than 0.2 where surface water shedding is important.

Splashing and bouncing cloud droplets should not account for any significant flow over the surface at below-freezing conditions. Nevertheless, some splashing and perhaps some bouncing have been noted in a few photographic frames. Many more closeup grazing-angle stop-action still photos are required to be statistically sure that the effect of bouncing and splashing can be ignored.

Some closeup grazing-angle movie and still data should be obtained in a few natural icing flight encounters for the following reasons. In a flight through a natural icing cloud the LWC varies greatly with time, whereas the IRT cloud is essentially steady. It is therefore possible that the time period of initial surface droplet flow will be a much larger fraction of the total icing time in an icing flight than it is in the IRT, especially with a large airfoil.

CONCLUDING REMARKS

The physical model for ice accretion at high airspeeds needs modifications. Some of these suggested modifications are as follows:

1. The closeup movies and still photos of the icing process that were obtained in these experiments show that at aircraft airspeeds there is no surface flow of water after a short initial flow.
2. The conventional freezing-fraction concept is physically wrong for aircraft airspeeds because there is no liquid flow over the ice surfaces after a short period of time. The conventional freezing fraction might still be a reasonable approximation for low airspeeds or near the freezing temperature because the initial flow lasts for a much longer time.
3. The freezing fraction needs to be replaced by a more correct but complex transient process involving the large rapid increase in the heat transfer coefficient for rough glaze ice. In addition there is an initial flow of large surface drops which tend to shed if they are big enough. This initial flow stops because of the greatly increased surface-tension adhesion to the rough ice surface. The momentum and mass balances for any water on the ice surface

are strongly coupled with the energy balance because the cloud droplet impact mass flux minus the freezing rate dictates how much water is available on the ice surface to make either the large surface drops (required by surface tension forces), a thin film, or rime ice.

4. The major cause of the different ice shapes (horn-glaze and rime ice) after the initial flow transient with its water shedding appears to be the gradual interactive bootstrap effect of the ice shape and the ice roughness on the local airflow and, therefore, the local droplet catch and heat transfer coefficient. The roughness of glaze and rime ice is quite different, even at the start of freezing, which effects the heat transfer coefficient. Glaze ice shapes are affected by the initial surface flow and also by shedding of the surface drops, especially near the freezing temperature. Shedding of ice must also be included in any ice accretion theory for all icing conditions at the high G forces of a rotor or at aircraft airspeeds.

REFERENCES

1. Lozowski, E.P.; Stallabrass, J.R.; and Hearty, P.F.: The Icing of an Unheated Non-Rotating Cylinder in Liquid Water Droplet: Ice Crystal Clouds. LTR-LT-96, National Research Council of Canada, Feb. 1979. (Avail. NTIS, AD-B069533.)
2. Ackley, S.F.; and Templeton, M.K.: Computer Modeling of Atmospheric Ice Accretion. CRREL-7904, Army Cold Regions Research and Engineering Lab, Mar. 1979. (Avail. NTIS, AD-A068582.)
3. MacArthur, C.D.: Numerical Simulation of Airfoil Ice Accretion. AIAA Paper 83-0112, Jan. 1983.
4. Olsen, W.; and Newton, J.: Experimental Evaluation of Existing Icing Scaling Laws, A Progress Report. AIAA Paper 85-0470, Jan. 1985. (NASA TM-88973.)
5. Ruff, G.A.: Analysis and Verification of the Icing Scaling Equations. Vol. 1, AEDC-TR-85-30-vol-1, 1985. (Avail. NTIS, AD-A167976.)
6. Messinger, B.L.: Equilibrium Temperature of an Unheated Icing Surface as a Function of Airspeed. Aeronaut. Sci., vol. 20, no. 1, Jan. 1953, pp. 29-42.
7. Olsen, W.; Walker, E.; and Sotos, R.: Closeup Motion Picture Studies Showing Droplet Freezing Process of Aircraft Icing. NASA Movie C-313, 1985.
8. Olsen, W.; Takeuchi, D.; and Adams, K.: Experimental Comparison of Icing Cloud Instruments. AIAA Paper 83-0026, Jan. 1983. (NASA TM-83340.)
9. Walker, E.D.; and Slater, H.A.: Method of Reducing Temperature in High-Speed Photography. NASA TM-83620, 1984.
10. Bikerman, J.J.: Sliding of Drops from Surfaces of Different Roughness. Colloid. Sci., vol. 5, 1950, pp. 349-359.

11. Merte, H., Jr.; and Yamali, C.: Profile and Departure Size of Condensation Drops on Vertical Surfaces. *Warme-und Stoffubertragung*, vol. 17, 1983, pp. 171-180.
12. Steger, J.L.: Implicit Finite-Difference Simulation of Flow About Arbitrary Two-Dimensional Geometries. *AIAA J.*, vol. 16, no. 7, July 1978, pp. 679-686.
13. Stallabrass, R.: An Appraisal of the Single Rotating Cylinder Method of Liquid Water Content. LTR-LT-92, National Research Council of Canada, 1978.
14. Olsen, W.; Shaw, R.; and Newton, J.: Ice Shapes and the Resulting Drag Increase for a NACA 0012 Airfoil. *AIAA Paper 84-0109*, Jan. 1984. (NASA TM-83556.)
15. Van Fossen, G.J., et al: Heat Transfer Distributions Around Nominal Ice Accretion Shapes Formed on a Cylinder in the NASA Lewis Icing Research Tunnel. *AIAA Paper 84-0017*, Jan. 1984. (NASA TM-83557.)

TABLE I. - CONDITIONS OF FILM SEQUENCES OF THE FILM SUPPLEMENT

[All sequences at 24 frames/sec and start at beginning of cloud droplet impingement.]

(a) Above-freezing flow over airfoil surface

| Film roll number | Film sequence number | Position viewed along surface, s, mm | Icing tunnel conditions | | | | Stagnation line freezing fraction |
|--|----------------------|--------------------------------------|---------------------------|--------------------|--------------------|-----------------------------|-----------------------------------|
| | | | Total air temperature, °C | Airspeed, V, km/hr | Drop size, MVD, μm | Local LWC, g/m ³ | |
| Stagnation region | | | | | | | |
| 1 | a ₁ | 0 (Stag.) | 5 | 320 | 30 | 0.48 | 0 |
| Downstream of stagnation region | | | | | | | |
| 1 | 2 | 9 | 5 | 320 | 30 | 0.48 | 0 |
| 1 | 3 | 15 | 5 | 320 | 30 | .48 | 0 |
| 1 | 4 | 21 | 5 | 320 | 30 | .48 | 0 |
| Over rough simulated ice made of plastic | | | | | | | |
| 1 | 5 | Stag. | 5 | 320 | 30 | 0.48 | 0 |
| Effect of drop size at constant airspeed | | | | | | | |
| 1 | b ₆ | 0 | 5 | 320 | 30 | 0.48 | 0 |
| 1 | 7 | Stag. | 5 | 320 | 15 | .25 | 0 |
| Effect of airspeed at constant drop size and LWC•V | | | | | | | |
| 1 | 7 | Stag. | 5 | 320 | 15 | 0.25 | 0 |
| 1 | 8 | Stag. | 5 | 160 | 15 | .48 | 0 |
| 1 | 9 | Stag. | 5 | 50 | 15 | 1.6 | 0 |

^aSequences used in NASA Film C-313.

^bSame as film sequence 1.

TABLE I. - Continued.

(b) Ice growth and surface flow below freezing

| Film roll number | Film sequence number | Position viewed along surface, s, mm | Icing tunnel conditions | | | | Stagnation line freezing fraction |
|--|----------------------|--------------------------------------|---------------------------|--------------------|--------------------|-----------------------------|-----------------------------------|
| | | | Total air temperature, °C | Airspeed, V, km/hr | Drop size, MVD, μm | Local LWC, g/m ³ | |
| Stagnation region, vary temperature at 30 μm and 320 km/hr | | | | | | | |
| 1 | a ₁₀ | Stag. | -1.1 | 320 | 30 | 0.48 | 0.20 |
| 1 | a ₁₁ | ↓ | -3 | ↓ | ↓ | ↓ | .28 |
| 2 | a ₁₂ | ↓ | -7 | ↓ | ↓ | ↓ | .47 |
| 2 | a ₁₃ | ↓ | -12 | ↓ | ↓ | ↓ | .70 |
| 2 | a ₁₄ | ↓ | -18 | ↓ | ↓ | ↓ | .94 |
| Stagnation region, vary temperature at 15 μm and 320 km/hr | | | | | | | |
| 2 | a ₁₅ | Stag. | -1.7 | 320 | 15 | 0.25 | 0.39 |
| ↓ | 16 | ↓ | -3 | ↓ | ↓ | ↓ | .56 |
| ↓ | 17 | ↓ | -7 | ↓ | ↓ | ↓ | .93 |
| ↓ | 18 | ↓ | -12 | ↓ | ↓ | ↓ | 1.4 |
| ↓ | 19 | ↓ | -18 | ↓ | ↓ | ↓ | 1.9 |
| Stagnation region, vary temperature at 15 μm and 160 km/hr; same LWC•V as sequences 15 to 19 above | | | | | | | |
| 3 | 20 | Stag. | -1.7 | 160 | 15 | 0.48 | 0.20 |
| ↓ | 21 | ↓ | -3 | ↓ | ↓ | ↓ | .35 |
| ↓ | 22 | ↓ | -7 | ↓ | ↓ | ↓ | .68 |
| ↓ | 23 | ↓ | -12 | ↓ | ↓ | ↓ | 1.08 |
| ↓ | 24 | ↓ | -18 | (b) | (b) | ↓ | 1.4 |
| Stagnation region, vary temperature at 15 μm and 50 km/hr; same LWC•V as sequences 15 to 19 above | | | | | | | |
| 3 | a ₂₅ | Stag. | -2 | 50 | 15 | 1.6 | 0.17 |
| 3 | 26 | ↓ | -4 | ↓ | ↓ | ↓ | .28 |
| 4 | 27 | ↓ | -7 | ↓ | ↓ | ↓ | .50 |
| 4 | 28 | ↓ | -12 | ↓ | ↓ | ↓ | .82 |
| 4 | 29 | ↓ | -18 | (b) | (b) | ↓ | 1.6 |
| Along airfoil surface at -1 °C | | | | | | | |
| 4 | 30 | 0 | -1.1 | 320 | 30 | 0.48 | 0.20 |
| ↓ | 31 | (Stag.) | -1.7 | ↓ | ↓ | ↓ | ↓ |
| ↓ | 32 | 9 | -1.7 | ↓ | ↓ | ↓ | ↓ |
| ↓ | 33 | 15 | -1.7 | ↓ | ↓ | ↓ | ↓ |
| ↓ | | 21 | -1.7 | ↓ | ↓ | ↓ | ↓ |
| Along airfoil surface at -3 °C | | | | | | | |
| 4 | 34 | 0 | -3 | 320 | 30 | 0.48 | 0.28 |
| ↓ | 35 | (Stag.) | ↓ | ↓ | ↓ | ↓ | ↓ |
| ↓ | 36 | 9 | ↓ | ↓ | ↓ | ↓ | ↓ |
| 5 | 37 | 15 | ↓ | ↓ | ↓ | ↓ | ↓ |
| 5 | | 21 | ↓ | ↓ | ↓ | ↓ | ↓ |
| Along airfoil surface at -7 °C | | | | | | | |
| 5 | 38 | 0 | -7 | 320 | 30 | 0.48 | 0.47 |
| ↓ | 39 | 9 | ↓ | ↓ | ↓ | ↓ | ↓ |
| ↓ | 40 | 15 | ↓ | ↓ | ↓ | ↓ | ↓ |
| ↓ | 41 | 21 | ↓ | ↓ | ↓ | ↓ | ↓ |
| Spray on, off, and on cycle | | | | | | | |
| 5 | 42 | 9 | -7 | 320 | 30 | 0.48 | 0.47 |

^aSequences used in NASA Film C-313.

^bLens fogged.

TABLE II. - TIME WHEN EVENTS CAUSED BY FREEZING OCCUR IN THE STAGNATION REGION OF THE AIRFOIL SURFACE

[Cloud droplet size, MVD, 15 μm ; droplet mass flux $\text{LWC} \cdot \text{V} = 22.2 \text{ g/m}^2\text{-sec.}$]

| Film sequence | Airspeed, V, km/hr | Total temperature, °C | Calculated freezing fraction | Event caused by freezing | Time of event, sec | |
|---------------|--------------------|-----------------------|------------------------------|---|--------------------|--------|
| | | | | | Stagnation zone | Zone 3 |
| 15 | 320 ↓ | -1.7 | 0.39 | Big surface drops stop moving ^a | 1 | 1 |
| 16 | | -3 | .56 | Big surface drops stop moving ^a | 1 | 1 |
| 17 | | -7 | .93 | Big surface drops stop moving ^a | 1 | 1 |
| 18 | | -12 | 1.4 | No big drops ^b or ^c | (e) | (e) |
| 19 | | -18 | 1.9 | Rime ice ^b | (e) | (e) |
| 20 | 160 ↓ | -1.7 | 0.2 | Big drops continue to move ^d | (e) | (e) |
| 21 | | -3 | .35 | Big drops stop moving ^a | 6.5 | 14.5 |
| 22 | | -7 | .68 | Big drops stop moving ^a | 0 | 3 |
| 23 | | -12 | 1.08 | Film formed and starts moving ^c | 16.7 | 16.7 |
| 24 | | -18 | 1.4 | Film forms with a few big stationary drops. Film starts to flow. Rime ice ^b | 12.5 | 12.5 |
| 25 | 50 ↓ | -2 | 0.17 | Big drops continue to move ^d | (e) | (e) |
| 26 | | -4 | .28 | Big drops form, then thin film ^c | (e) | (e) |
| 27 | | -7 | .5 | Thin film starts to flow | 104 | 104 |
| 28 | | -12 | .82 | No big drops, but film on ice hills ^c | (e) | (e) |
| 29 | | -18 | 1.6 | Film thick enough to start to flow Film forms, but never flows ^c Rime ice ^b | 50 | 50 |

Ice description:

^aTime sequence shown by figures 9 and 13, involving big surface drop downstream of a thin liquid film in the stagnation region that is slowly taken over by big drops as layer thickens.

^bRime ice for whole sequence.

^cA thin film predominates for whole sequence with very few if any big drops. The water film slowly thickens over thickening rough ice layer and may get thick enough to flow.

^dBig drops grow then move when big enough and perhaps shed; this may occur through many cycles of growing and shedding while rough ice grows underneath.

^eEntire sequence.

TABLE III. - THE EFFECTS OF VARIED ICING CONDITIONS

- The biggest surface drops occur at low airspeeds.
- An initial flow of these big surface drops stops moving very quickly at high airspeeds (e.g., 320 km/hr) because rough ice forms rapidly and stops the drops. At low airspeeds or for large surfaces the freezing rate is slower so the initial flow of surface drops lasts longer.
- In the stagnation region, a thin water film forms which is wider and lasts longer at lower airspeeds and air temperatures.
- Rime ice forms at low air temperatures because droplets freeze before a large enough water layer can grow to form clear (glaze) ice.

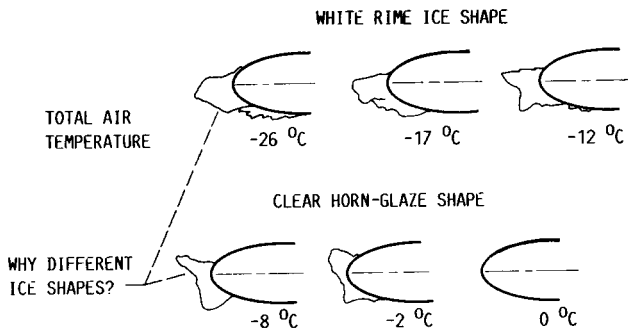


FIGURE 1. - EFFECT OF AIR TEMPERATURE ON ICE SHAPE. MVD, 20 μm ; LWC, 1.05 g/m^3 ; AIRSPEED, 338 km/hr ; TIME, 6.2 min ; 0.53-M-CHORD 0012 AIRFOIL AT 4° ANGLE OF ATTACK.

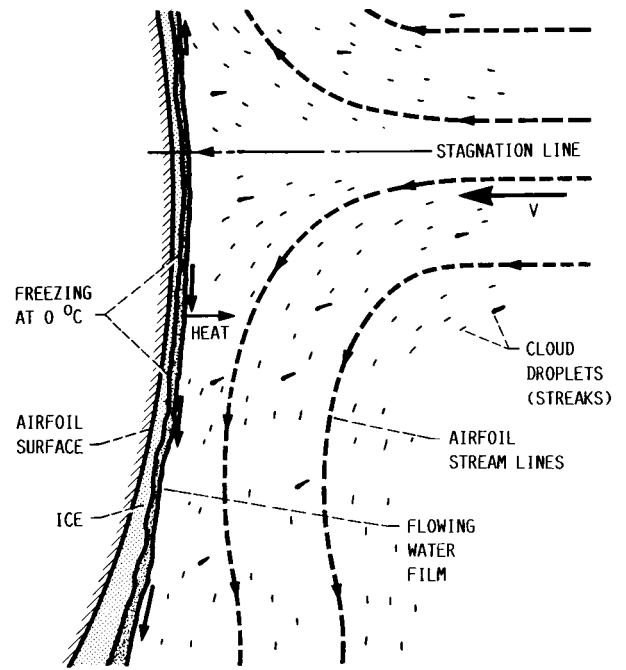
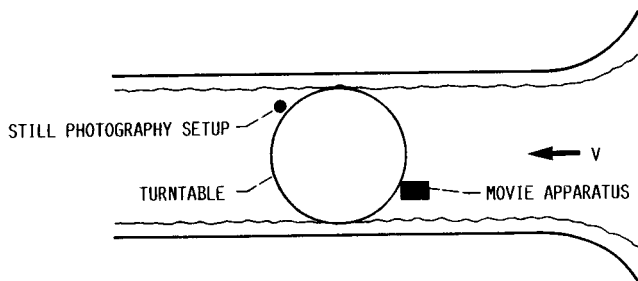
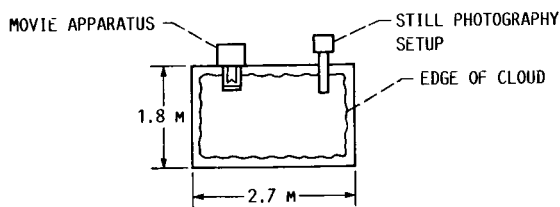


FIGURE 2. - EXISTING MODEL FOR ICING.



(A) TOP VIEW.



(B) LOOKING DOWNSTREAM.

FIGURE 3. - LOCATION OF THE MOVIE AND STILL PHOTOGRAPHY TEST SETUPS IN THE IRT TEST SECTION.

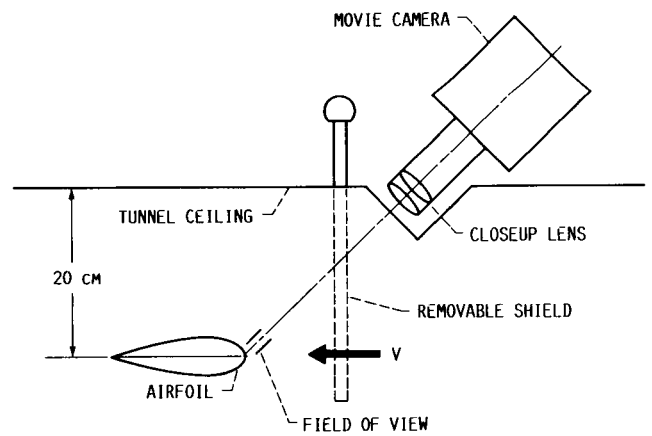


FIGURE 4. - SETUP FOR CLOSEUP MOVIES OF ICING PROCESS IN ICING RESEARCH TUNNEL.

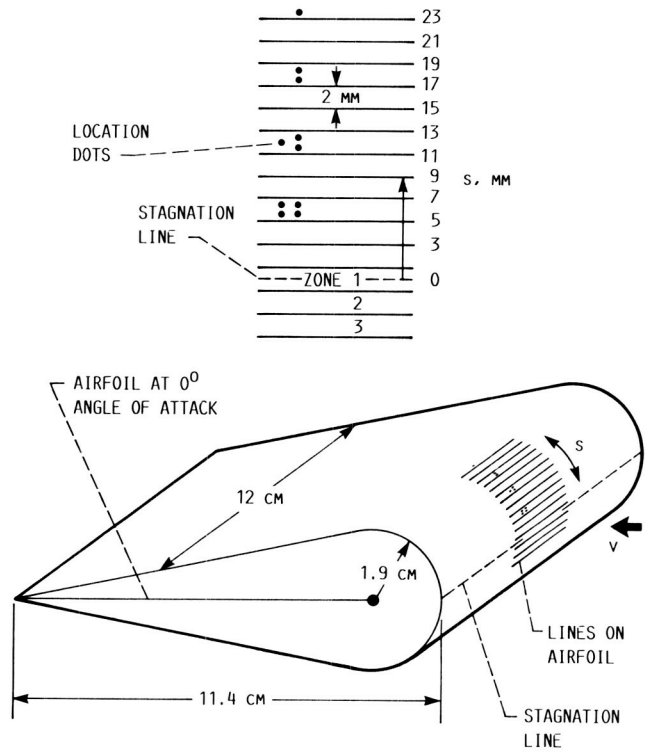


FIGURE 5. - SKETCH OF WOODEN AIRFOIL USED IN CLOSEUP MOVIES. DISTANCE ALONG AIRFOIL SURFACE FROM STAGNATION LINE, s , MM.

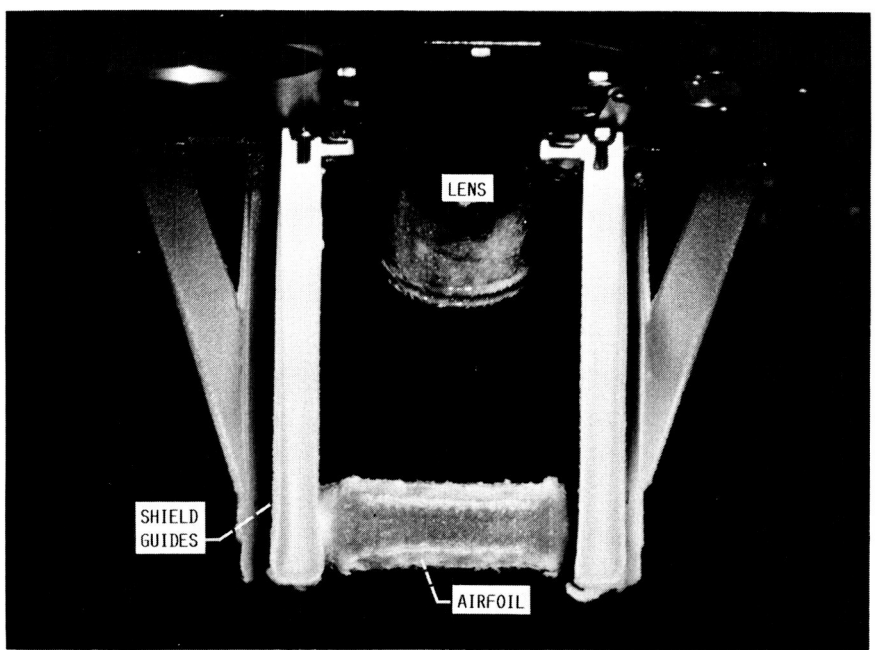


FIGURE 6. - CLOSEUP MOVIE APPARATUS LOOKING DOWNSTREAM AT AIRFOIL TO SHOW UNIFORM ICE ACCRETION.

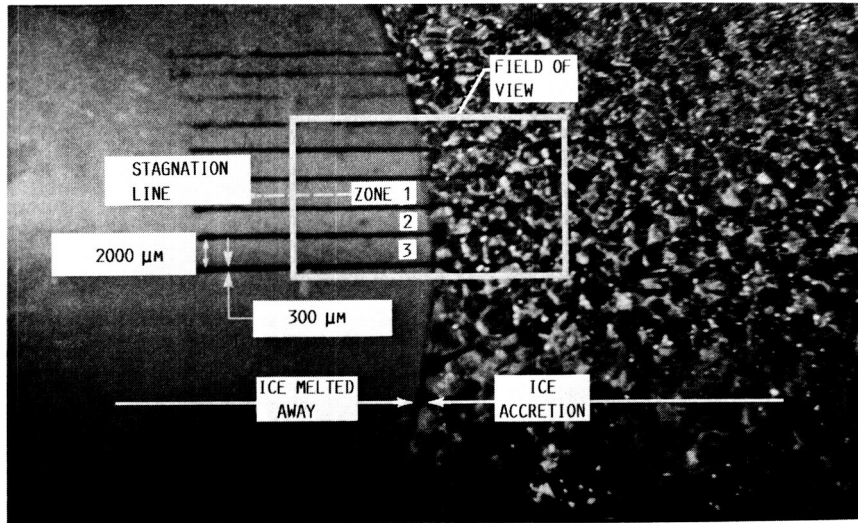
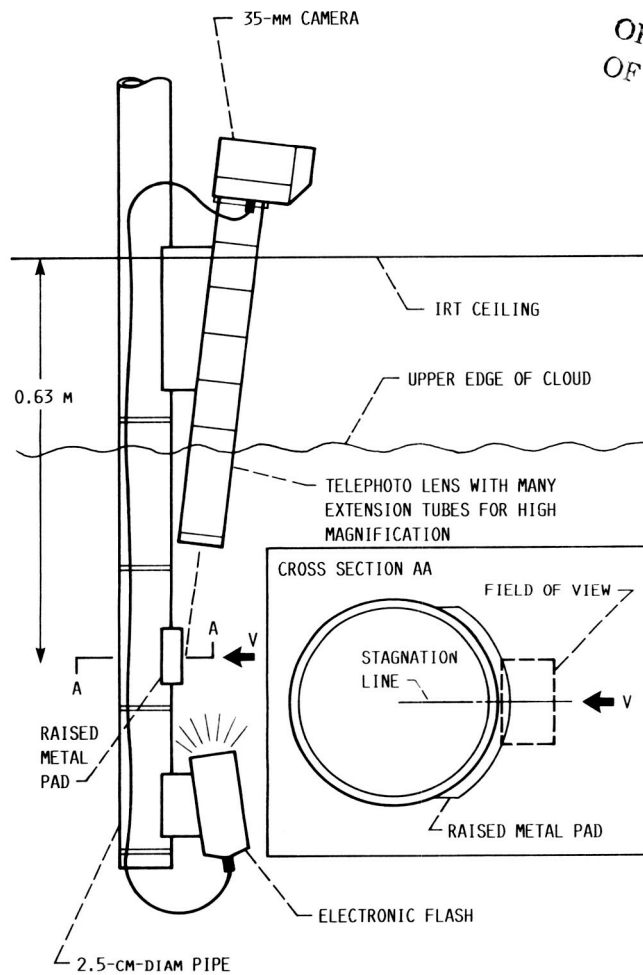
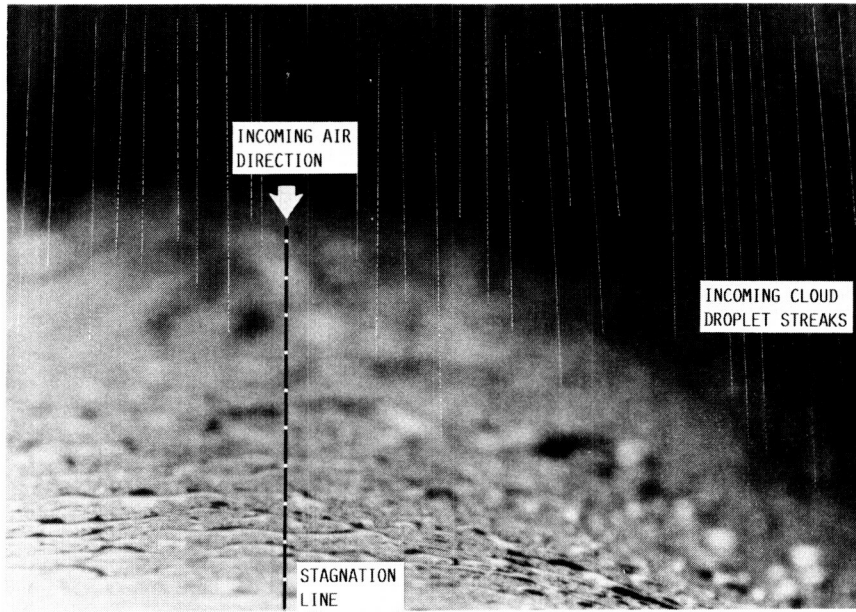


FIGURE 7. - AREA PHOTOGRAPHED.

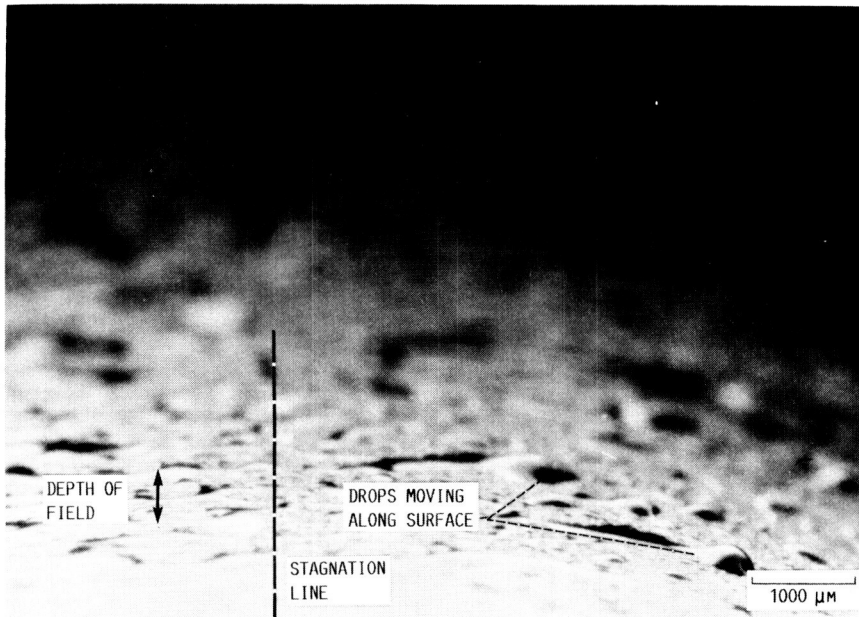


ORIGINAL PAGE IS
OF POOR QUALITY

FIGURE 8. - TEST SETUP FOR CLOSEUP GRAZING-ANGLE STILL PHOTOGRAPHS AT STOP-ACTION SPEEDS.



(A) SHORT TIME AFTER DRY SURFACE EXPOSED TO MICROSCOPIC CLOUD DROPLET IMPACTS AND BIG SURFACE DROPS GROW. (DROPLET STREAKS RETOUCHE FOR BETTER CLARITY IN PRINTING).

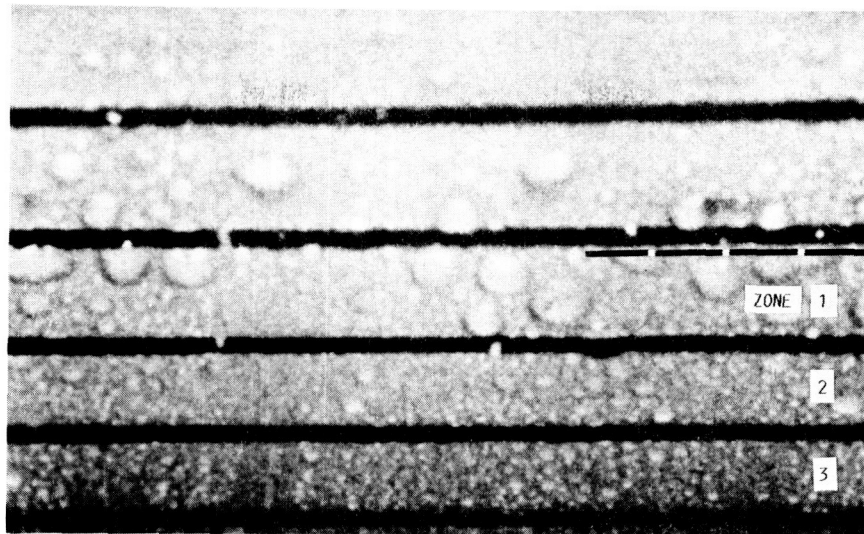


(B) SECONDS LATER WHEN A FEW SURFACE DROPS HAVE GROWN BIG ENOUGH TO MOVE ON SURFACE.

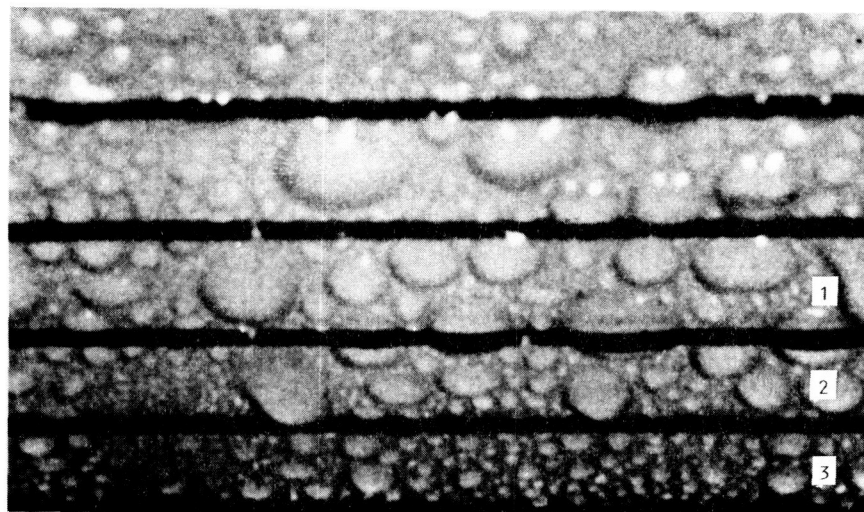
FIGURE 9. - CLOSEUP FLASH PICTURES AT GRAZING-ANGLE ALONG STAGNATION LINE OF 2.5-CM CYLINDER. AIR TEMPERATURE ABOVE FREEZING; EFFECTIVE EXPOSURE TIME, ABOUT 0.0001 SEC. MICROSCOPIC CLOUD DROPLETS (MVD = 30 μm) ARE SEEN AS STREAKS COMING IN WITH AIRFLOW FROM TOP OF PICTURE.

ORIGINAL PAGE IS
OF POOR QUALITY

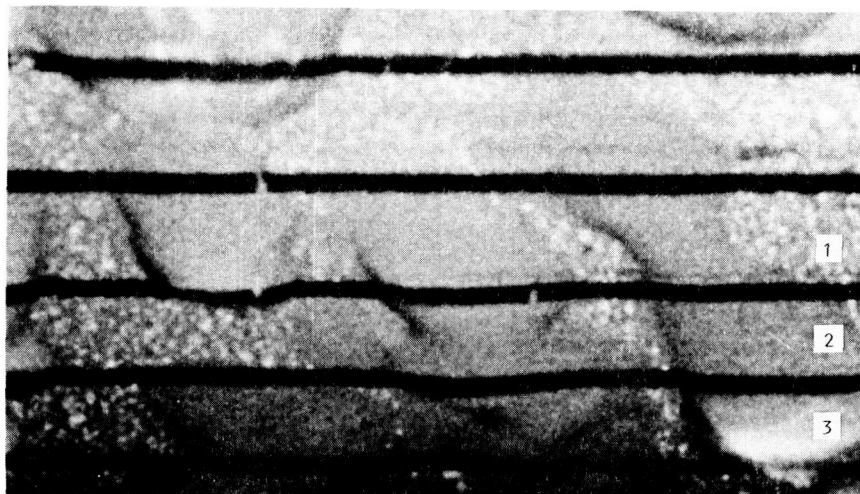
ORIGINAL PAGE IS
OF POOR QUALITY



(A) 320 KM/HR.



(B) 160 KM/HR.



(C) 50 KM/HR (JUST BEFORE THESE DROPS COALESCE INTO ONE BIG DROP AND SHED).

FIGURE 10. - SURFACE DROPS ABOVE FREEZING BEFORE FIRST SHED OVER A RANGE OF AIRPSEED. DROP SIZE, MVD, $15 \mu\text{m}$; LWC (V) = $80\ 000 \text{ g/M}^2 \text{ HR}$.

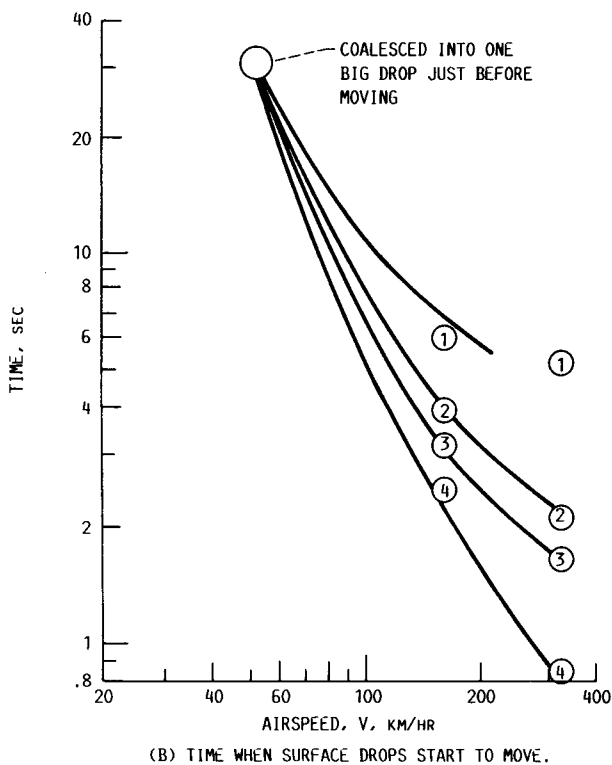
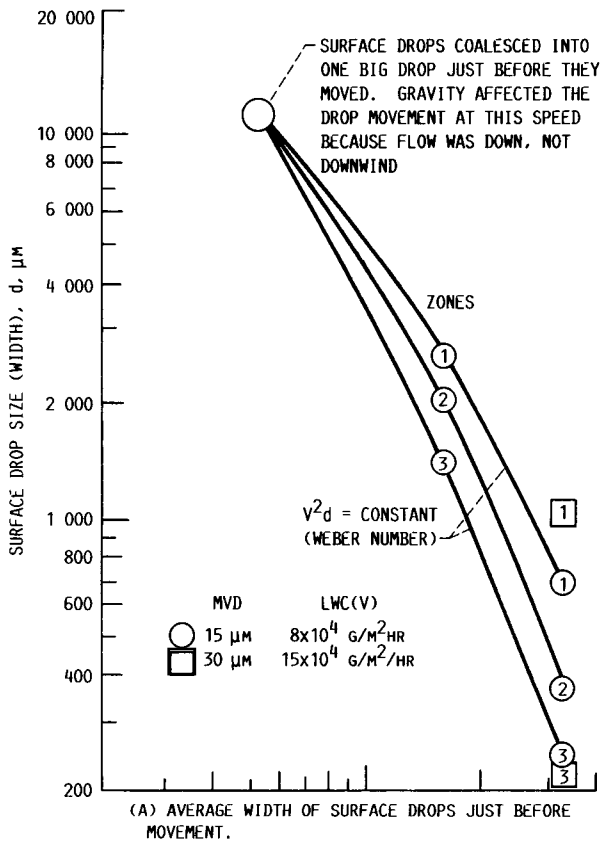


FIGURE 11. - ABOVE-FREEZING DATA ON DROP SIZE AND TIME WHEN SURFACE DROPS MOVE.

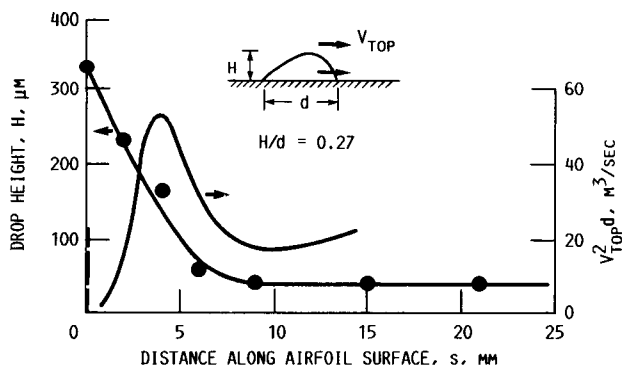
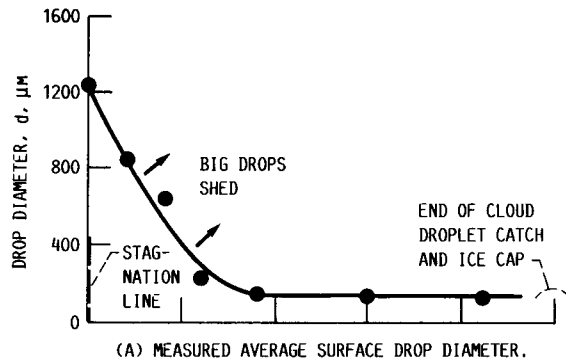


FIGURE 12. - EQUILIBRIUM SIZE OF DROPS ALONG AIRFOIL SURFACE AND FORCES ON DROPS FOR ABOVE-FREEZING CONDITIONS. AIR TEMPERATURE, $+5^\circ\text{C}$; AIRSPEED, 320 km/hr ; MVD, 30 μm ; LWC, 0.48 g/m^3 . (VARIATION OF DROP SIZE IS ± 40 PERCENT OF DROP DIAMETER d .)

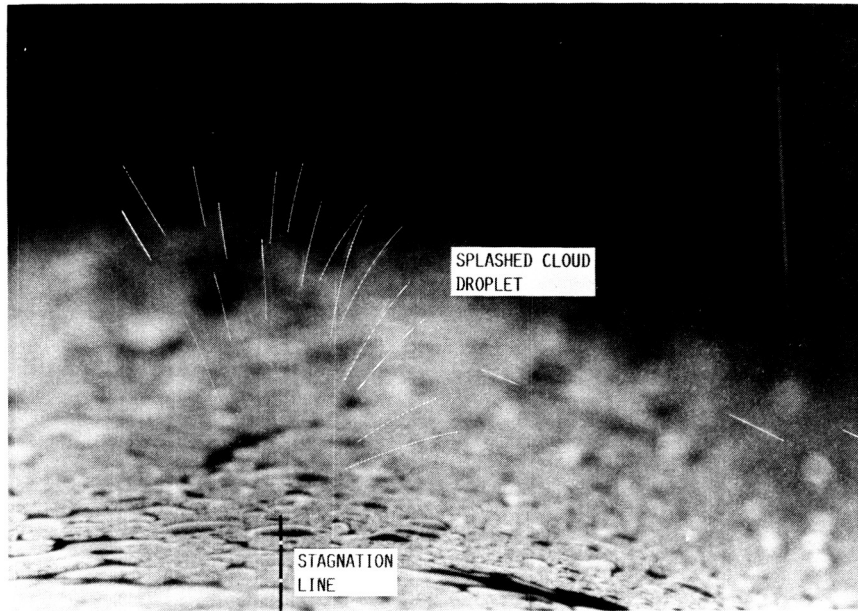


FIGURE 13. - RARE EVENT OF A SPLASHED CLOUD DROPLET; ABOVE-FREEZING CONDITIONS. (SPLASHED DROPLET STREAKS RETOUCHE FOR CLARITY IN PRINTING.)

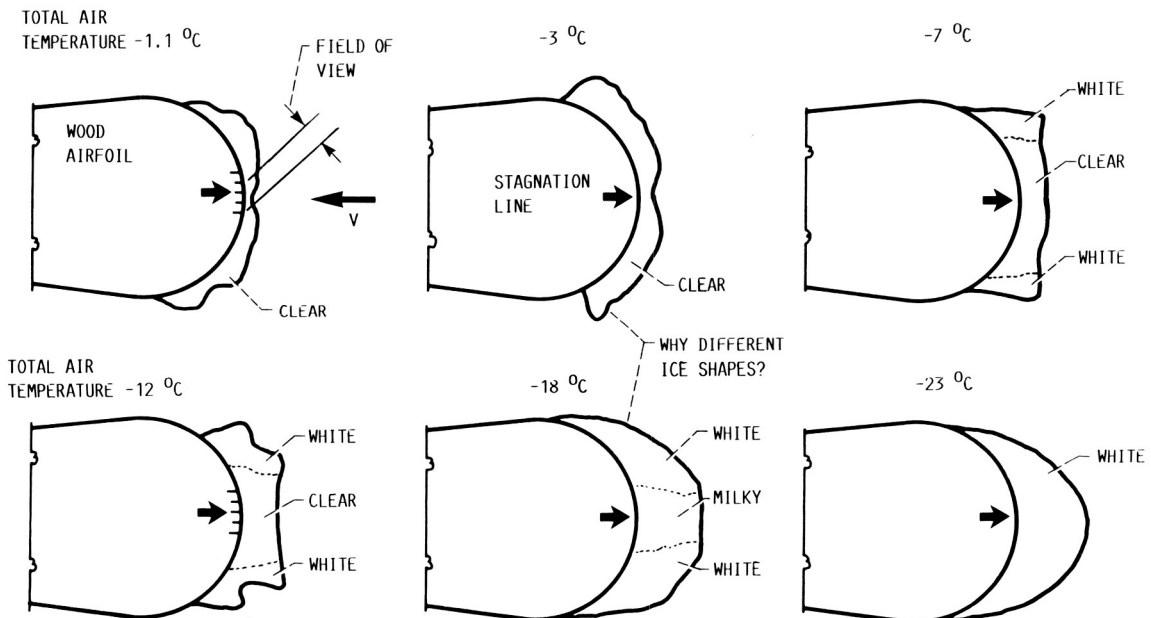
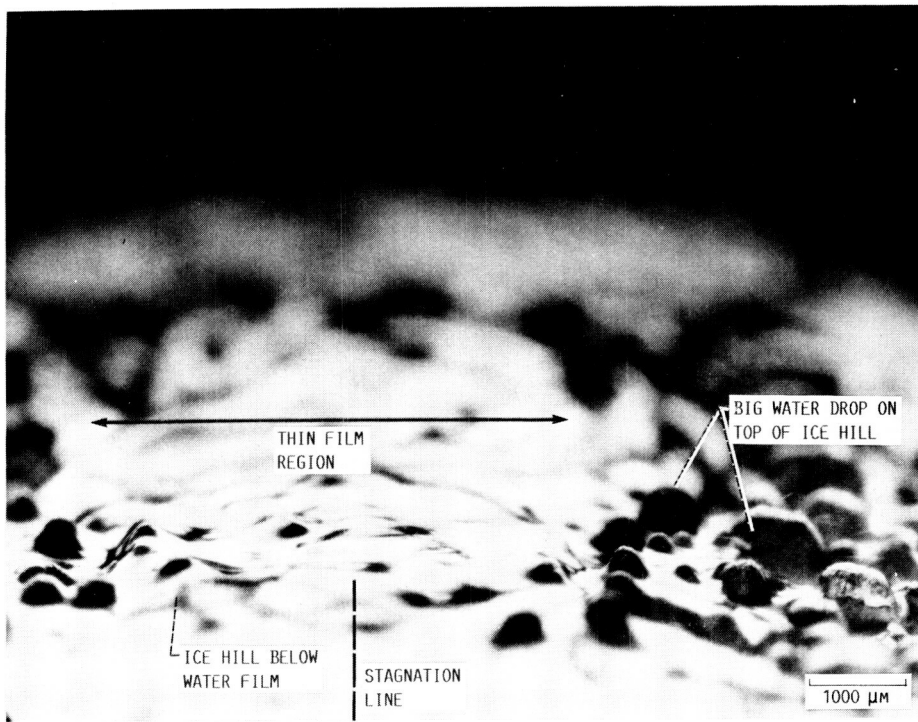
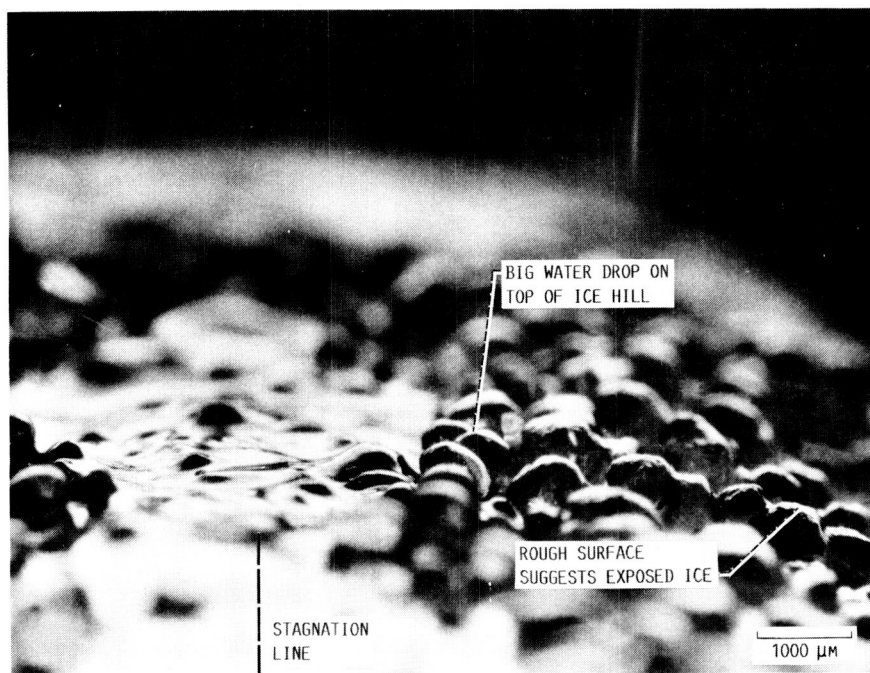


FIGURE 14. - ICE SHAPES AFTER 5-MIN SPRAY, AIRSPEED, 320 KM/HR; MVD, 30 μm ; LWC, 0.5 g/m^3 .



(A) 30 SEC.

FIGURE 15. - CLOSEUP GRAZING-ANGLE STILL PHOTOS OF ICE FORMED AT BELOW-FREEZING AIR TEMPERATURE OF -2°C .

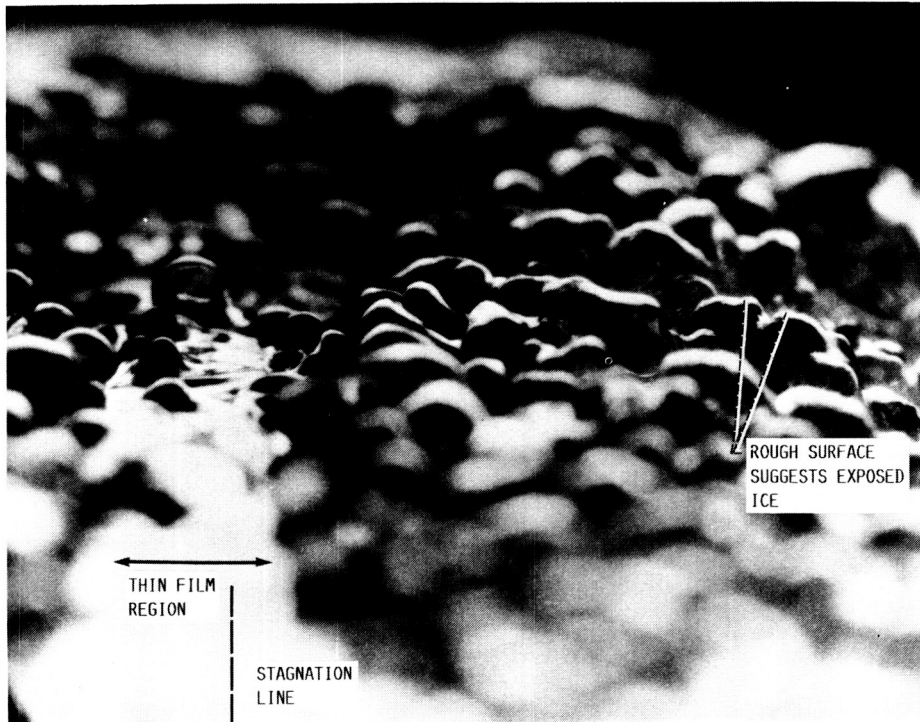


(B) 50 SEC.

FIGURE 15. - CONTINUED.

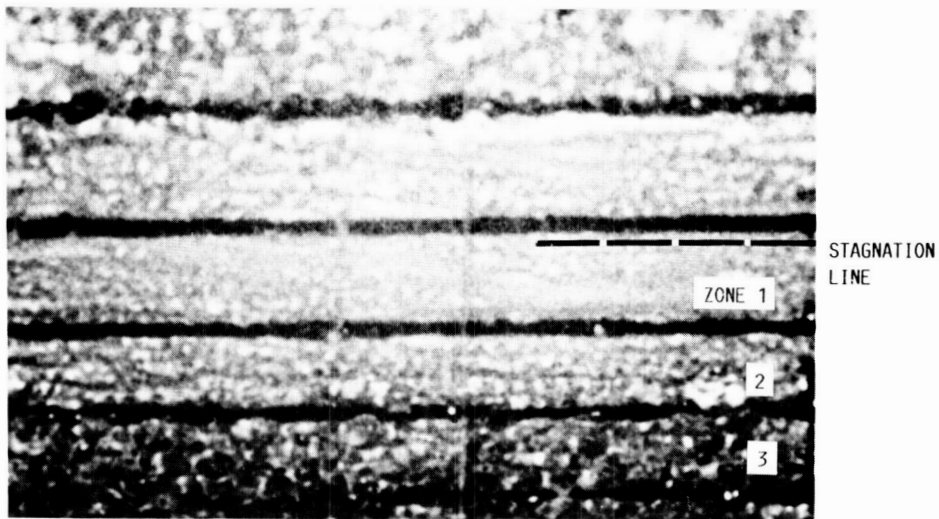
ORIGINAL PAGE IS
OF POOR QUALITY

ORIGINAL PAGE IS
OF POOR QUALITY

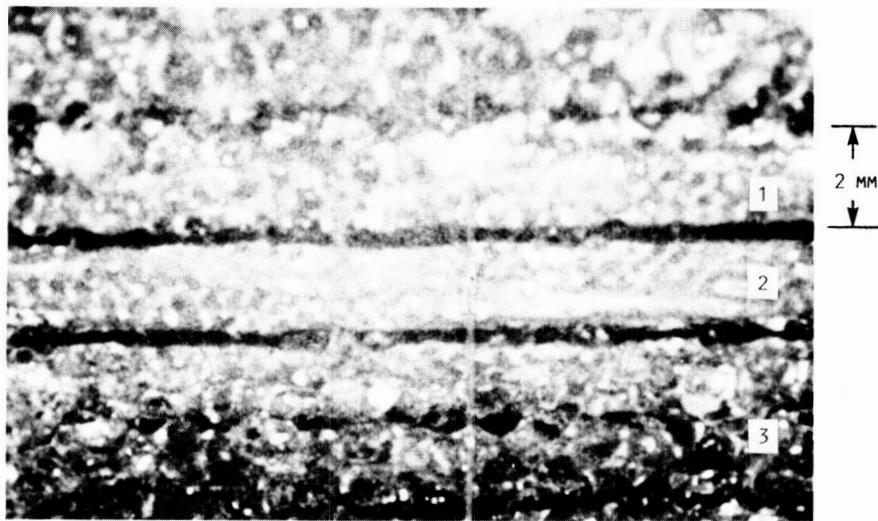


(C) 75 sec.

FIGURE 15. - CONCLUDED.



(A) 30 SEC.



(B) 50 SEC.



(C) 75 SEC.

FIGURE 16. - FRAMES FROM FILM SEQUENCE 11 THAT CLOSELY MATCH FIGURE 15.
 AIRSPEED, 320 KM/HR; MVD, 30 μ M; AIR TEMPERATURE, -3° C; LWC,
 0.48 G/M³. (VERTICAL LINE IS A SCRATCH IN MOVIE FILM.)



FIGURE 17. - MICROSCOPIC CLOUD DROPLETS COMING IN TO IMPACT AND FORM RIME ICE. TOTAL AIR TEMPERATURE, -26°C . (CLOUD DROPLET STREAKS RETOUCED FOR CLARITY IN PRINTING.)

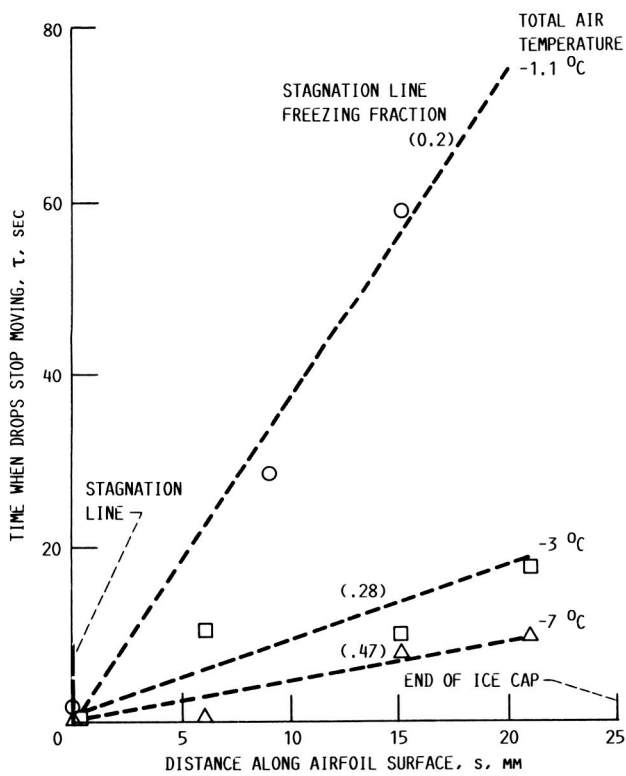


FIGURE 18. - TIME WHEN BIG SURFACE DROPS STOP MOVING ALONG AIRFOIL SURFACE BECAUSE OF FREEZING. CLOUD DROPLET SIZE, MVD, $30\ \mu\text{m}$; LWC, $0.48\ \text{g/m}^3$; AIRSPEED, $320\ \text{km/hr}$.

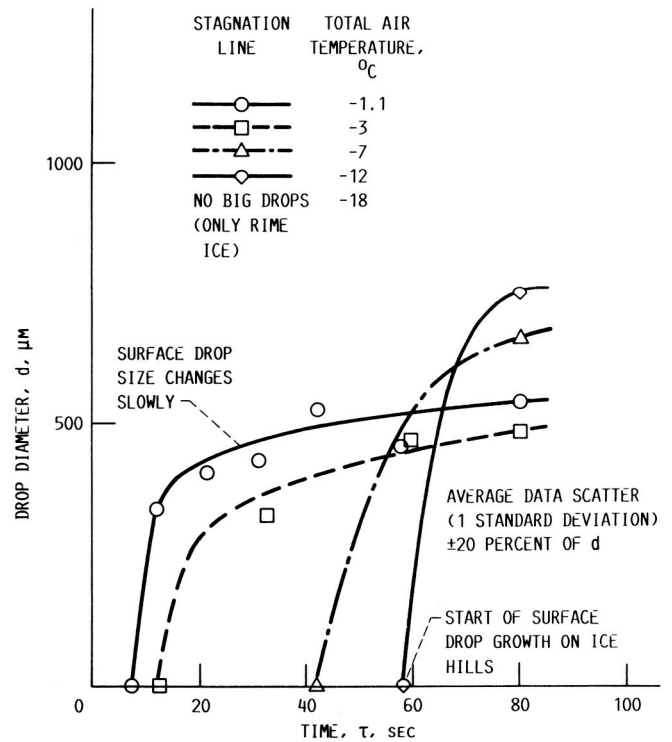


FIGURE 19. - GROWTH HISTORY OF BIG SURFACE DROPS BELOW FREEZING IN STAGNATION REGION. CLOUD DROPLET SIZE, MVD, $30\ \mu\text{m}$; LWC, $0.48\ \text{g/m}^3$; AIRSPEED, $320\ \text{km/hr}$.

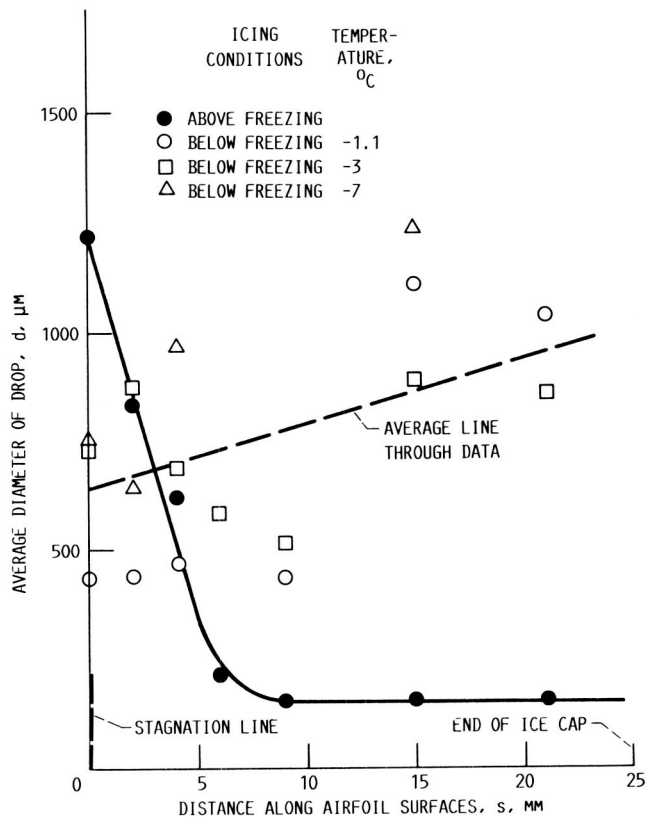


FIGURE 20. - LARGE-TIME SIZE OF SURFACE DROPS ALONG AIRFOIL SURFACE. CLOUD DROPLET SIZE, MVD, 30 μm; AIRSPEED, 320 km/hr; LWC, 0.48 g/m³. (AVERAGE SCATTER OF BELOW-FREEZING DATA IS ±33 PERCENT OF d.)

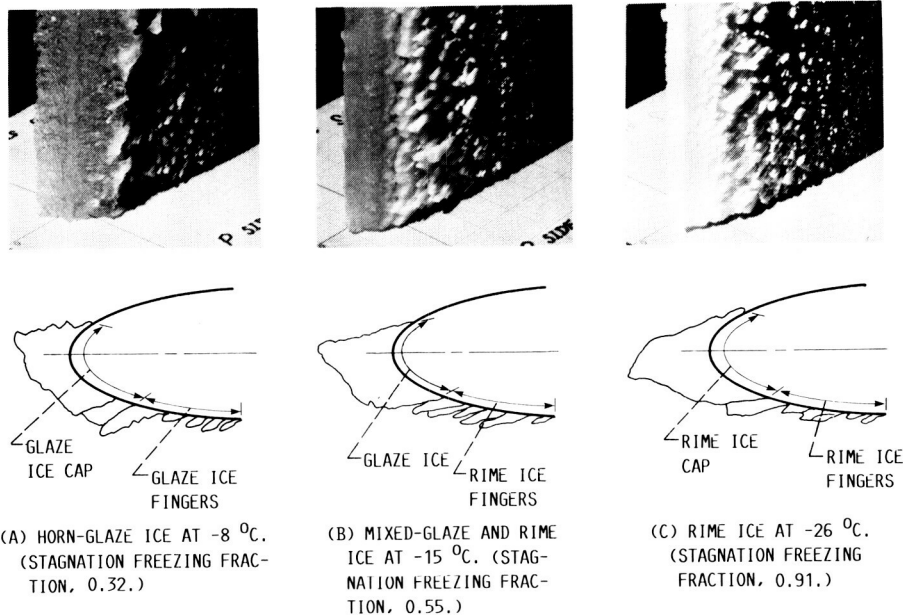
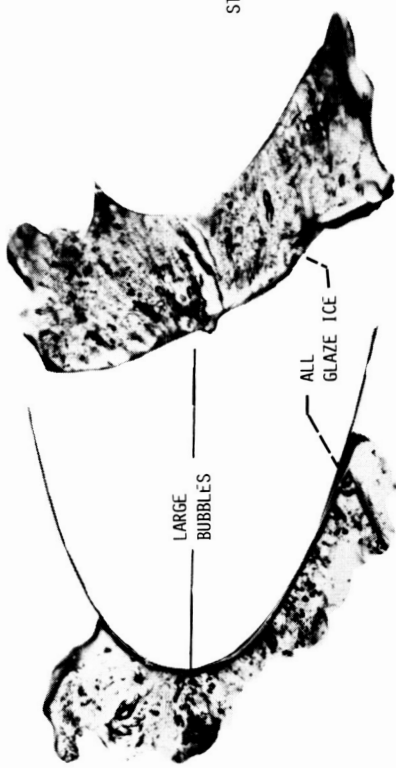


FIGURE 21. - ICE ACCRETION ON PRESSURE SIDE OF AIRFOIL. 0.53-M-CHORD 0012 AIRFOIL AT 4° ANGLE; LWC, 1.3 g/m³; TIME, 8 min; MVD, 20 μm; AIRSPEED, 209 km/hr.

ORIGINAL PAGE IS
OF POOR QUALITY

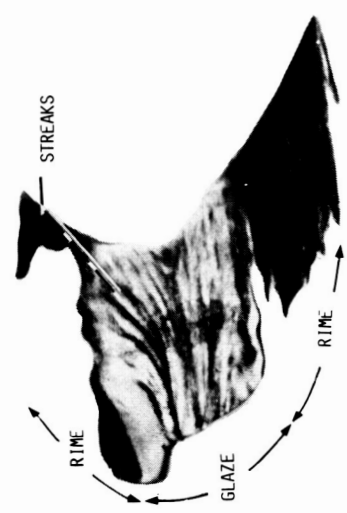


(A) TOTAL TEMPERATURE, -2°C
(STAGNATION FREEZING FRACTION, 0.22).

(B) TOTAL TEMPERATURE, -8°C
(STAGNATION FREEZING FRACTION, 0.32).

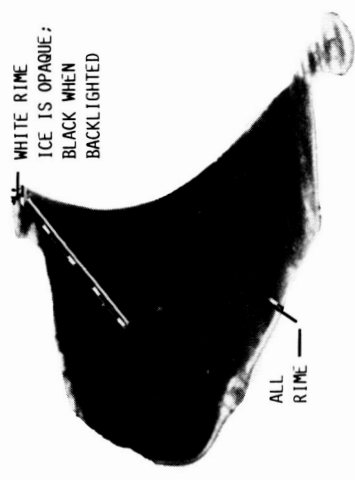


(C) TOTAL TEMPERATURE, -15°C
(STAGNATION FREEZING FRACTION, 0.55).



(D) TOTAL TEMPERATURE, -18°C
(STAGNATION FREEZING FRACTION, 0.65).

ORIGINAL PAGE IS
OF POOR QUALITY



(E) TOTAL TEMPERATURE, -26°C
(STAGNATION FREEZING FRACTION, 0.9).

FIGURE 22 - EFFECT OF TEMPERATURE ON ICE STRUCTURE. THIN ICE SAMPLES REMOVED FROM THE AIRFOIL AND BACKLIGHTED. AIRSPEED, 209 KM/HR; LMC, 1.5 g/m^3 ; MVD, $20 \mu\text{m}$; TIME, 8 MIN; 0.53-M-CHORD 0012 AIRFOIL AT 4° ANGLE.



(A) GLAZE ICE (LARGE CRYSTALS).

(B) RIME ICE (SMALL CRYSTALS).

FIGURE 23. - ICE CRYSTAL SIZE USING POLARIZED LIGHT.

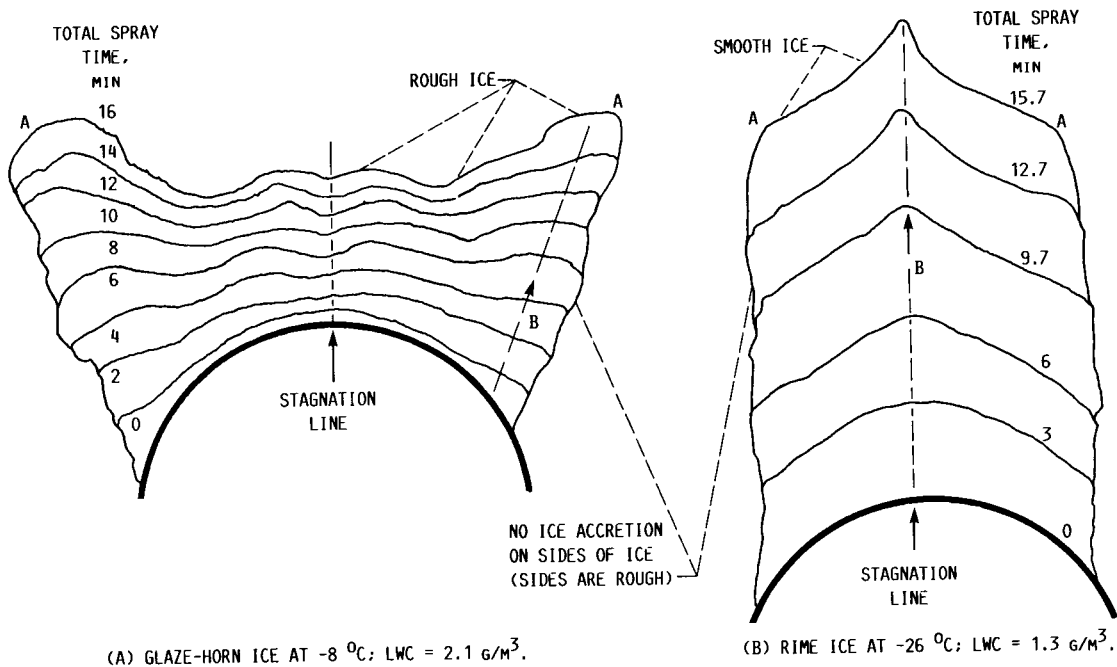


FIGURE 24. - DYE GROWTH RINGS FOR HORN-GLAZED AND RIME ICE SHAPES. AIRSPEED, 209 KM/HR; MVD, $20 \mu\text{m}$; 5.2-CM-DIAM CYLINDER. (DYE GROWTH RINGS SHOWN WERE TRACED FROM PHOTOGRAPHS.)

ORIGINAL PAGE IS
OF POOR QUALITY

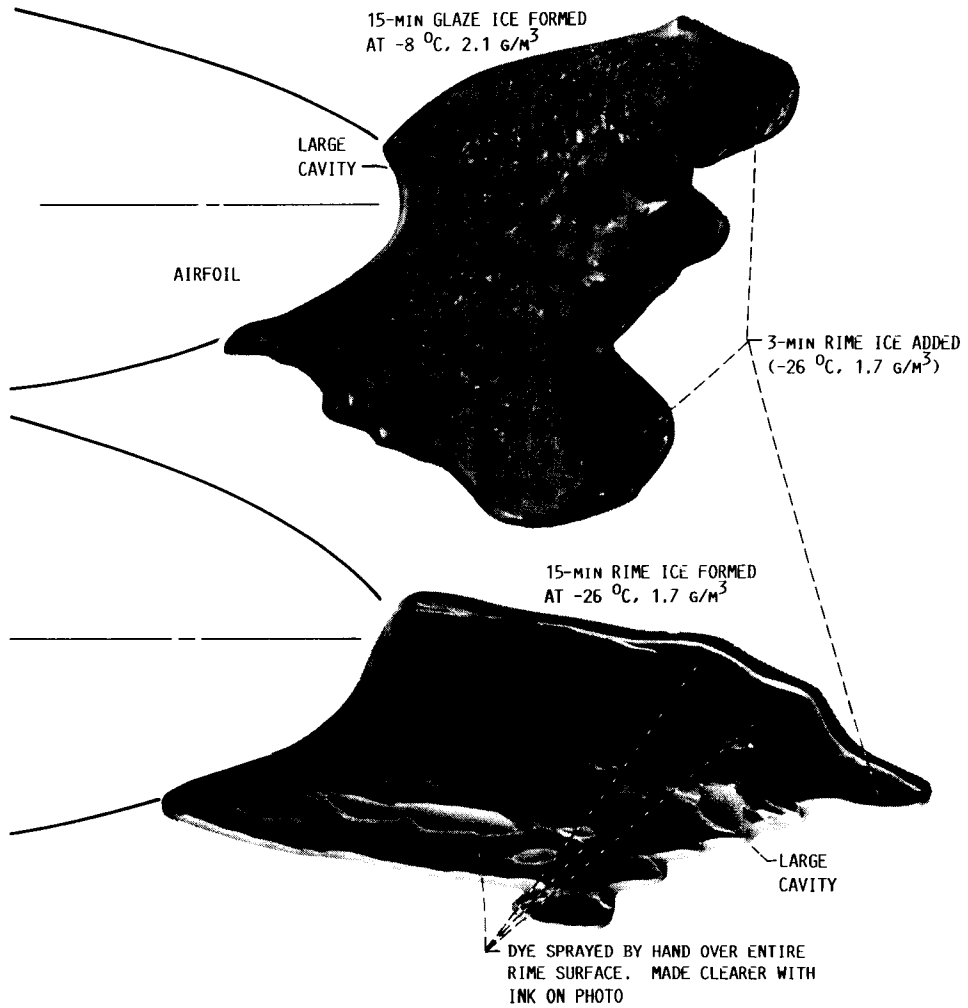


FIGURE 25. - EFFECT OF ICE SHAPE ON DROPLET CATCH. BACKLIGHTED THIN ICE SAMPLE OF 3-MIN RIME SPRAY ON TOP OF INITIAL ICE SHAPE. FOR ALL SPRAYS: MVD, $20 \mu\text{m}$; AIRSPEED, 209 KM/HR.

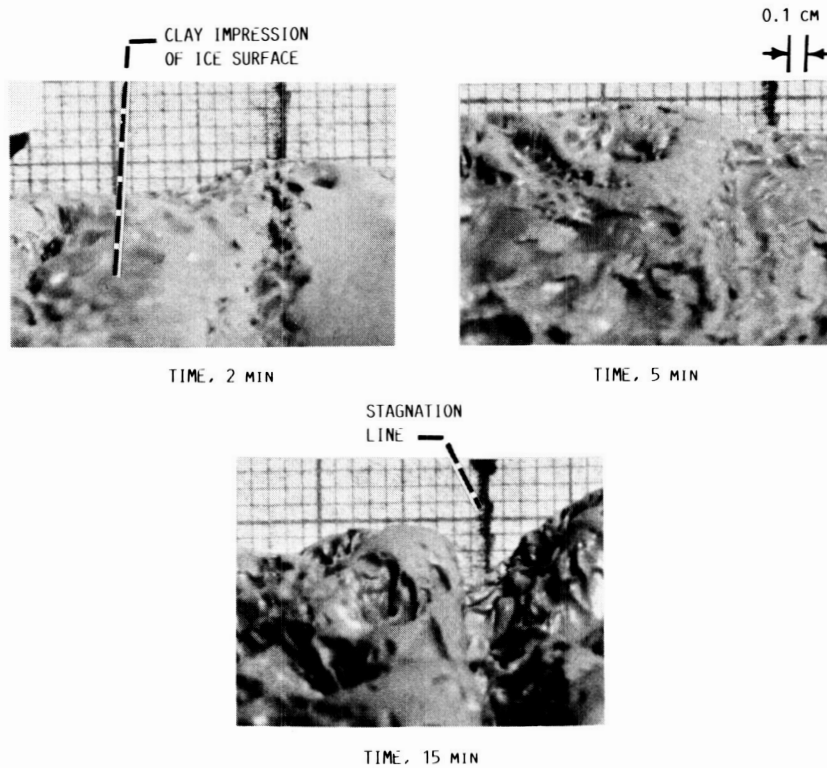


FIGURE 26. - EFFECT OF TIME ON ROUGHNESS OF ICE SURFACE IN STAGNATION REGION. AIR-SPEED, 209 KM/HR; TOTAL TEMPERATURE, -8°C ; MVD, $20\ \mu\text{m}$; LWC, $2.1\ \text{G/M}^3$; AIRFOIL, 0.53-M-CHORD 0012 AIRFOIL AT 4° ANGLE OF ATTACK.

ORIGINAL PAGE IS
 OF POOR QUALITY

ORIGINAL PAGE IS
OF POOR QUALITY

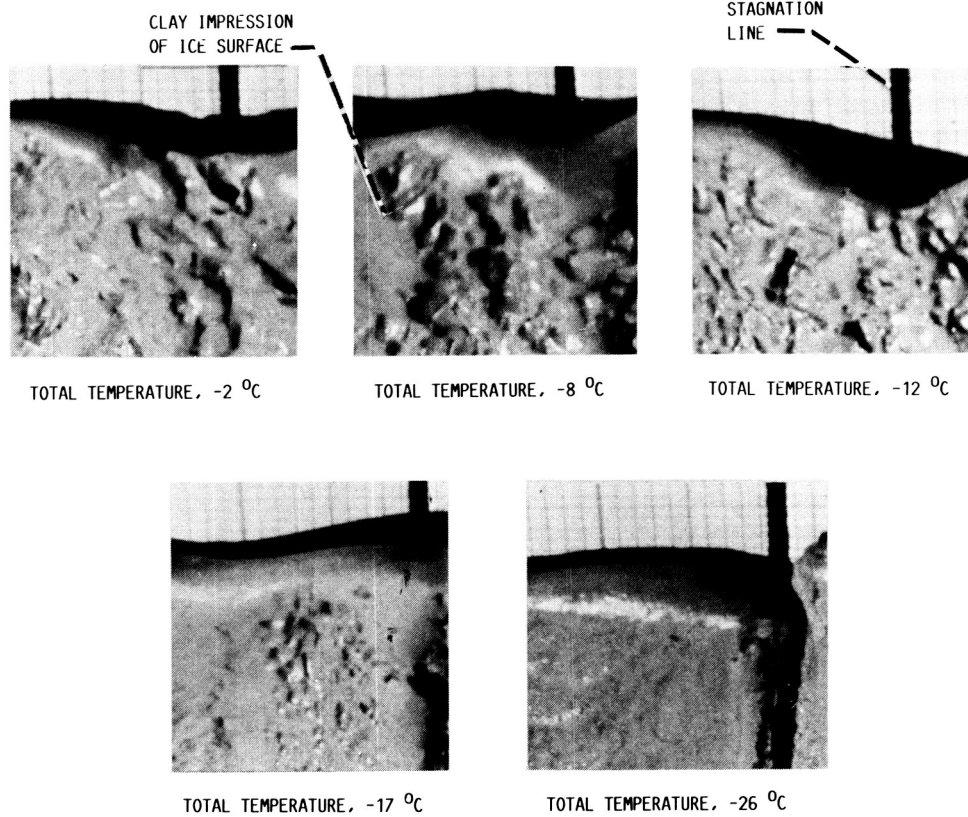


FIGURE 27. - EFFECT OF TEMPERATURE ON ROUGHNESS OF ICE SURFACE IN STAGNATION REGION; AIRSPEED, 338 KM/HR; MVD, $20\ \mu\text{m}$; LWC, $1.05\ \text{G/M}^3$; TIME, 6.2 MIN; AIRFOIL, 0.53-M-CHORD 0012 AIRFOIL AT 4° ANGLE OF ATTACK.

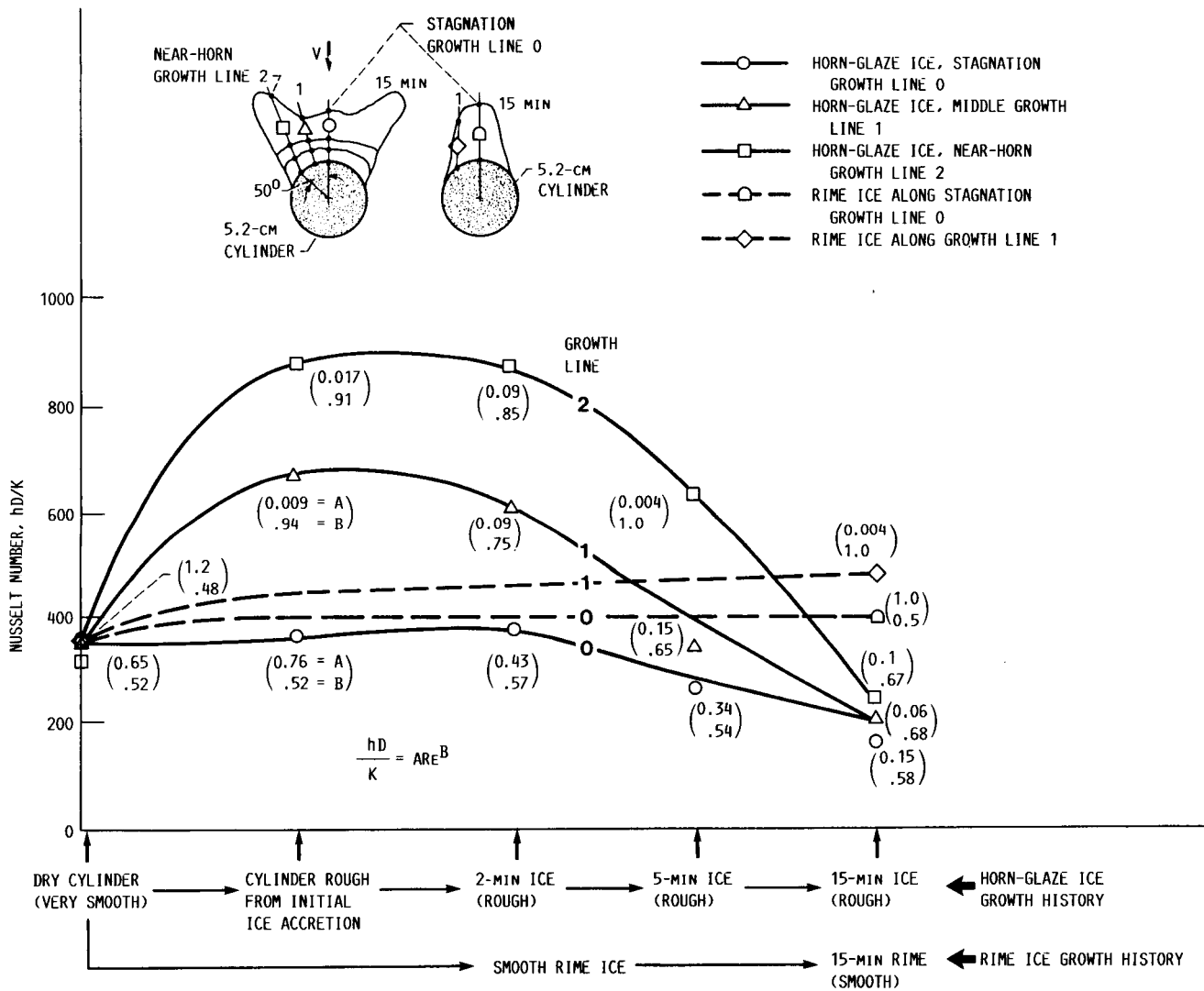
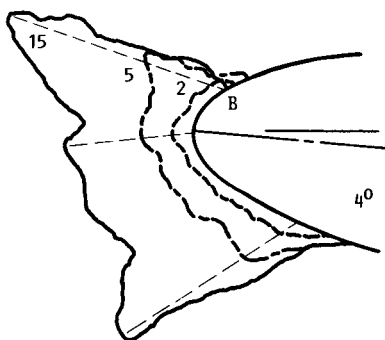
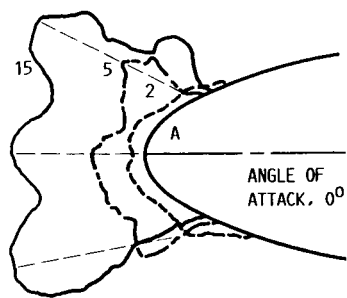


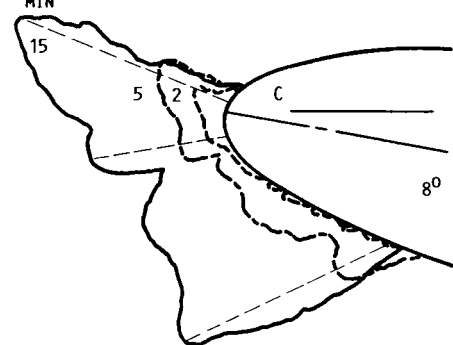
FIGURE 28. - CHANGE IN HEAT TRANSFER COEFFICIENT ALONG ICE GROWTH LINES AS ICE GROWS. CORRECTED $Re = 138\ 000$ (6.3-cm DRY CYLINDER Re CORRECTED TO AVERAGE Re FOR ICE ON 5.2-cm CYLINDER.) NUSSELT NUMBER DATA MEASURED BY VAN FOSSEN ON ARTIFICIAL ICE SHAPES WITH ARTIFICIAL ROUGHNESS.

| CASE | AIRSPEED, KM/HR | TEMPERATURE, °C | LWC, G/M ³ | MVD, μM | STAGNATION FREEZING FRACTION |
|-------|--------------------|--------------------|--------------------------|------------|---------------------------------|
| A,B,C | 209 | -8 | 2.1 | 20 | 0.24 |
| D,E,F | 209 | -26 | 1.0 | 12 | 1.08 |

GLAZE ICE



ACCRETION TIME,
MIN



RIME ICE

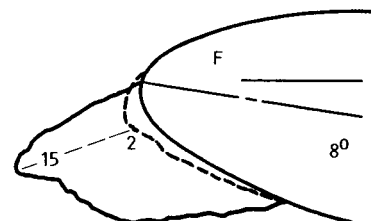
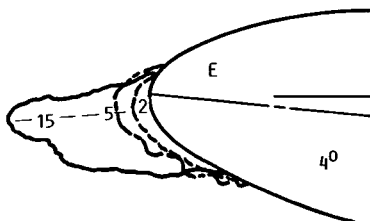
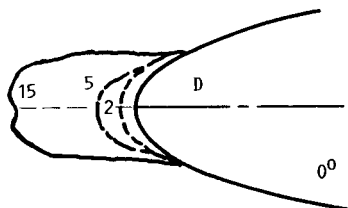


FIGURE 29. - EFFECT OF ACCRETION TIME AND AIRFOIL ANGLE OF ATTACK ON ICE SHAPE; 0.53-M-CHORD 0012 AIRFOIL.

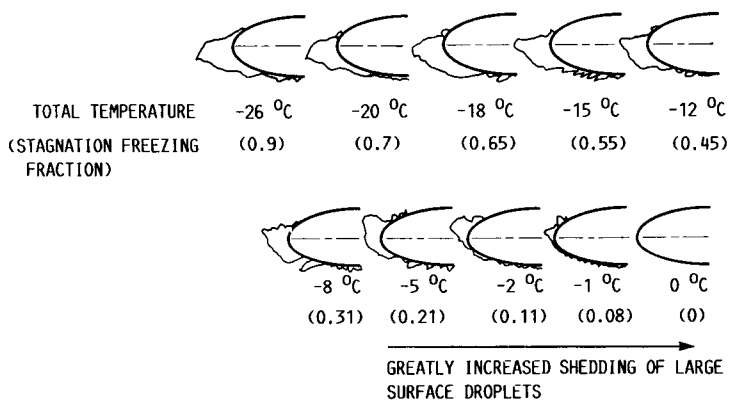
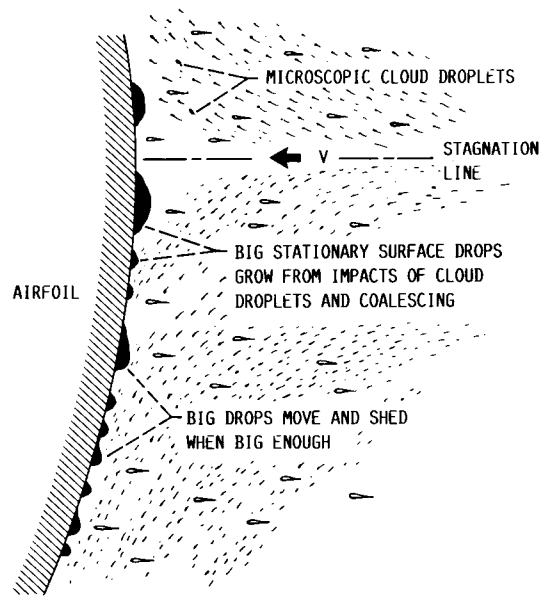
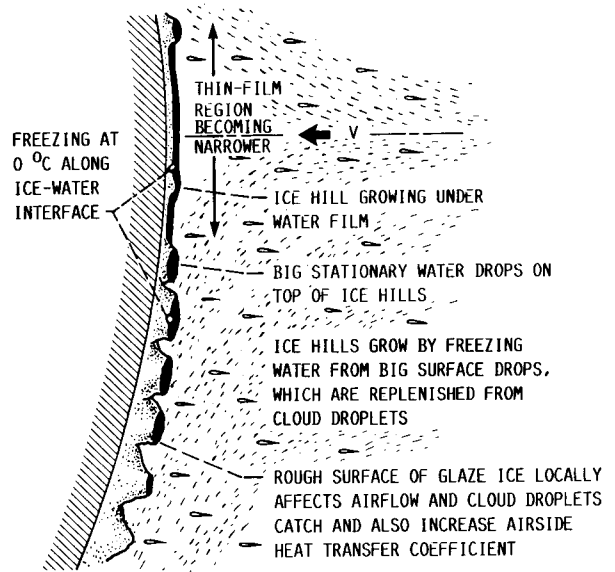


FIGURE 30. - EFFECT OF AIR TEMPERATURE ON ICE SHAPE AND SHEDDING.
 (OTHER PARAMETERS ALL CONSTANT: AIRSPEED, 209 KM/HR; LWC, 1.3 G/M³; MVD, 20 μM; TIME, 8 MIN; AIRFOIL AT 4°.)



(A) NO FREEZING OCCURRING (ABOVE 0 °C OR BEFORE FREEZING STOPS SURFACE DROPS).



(B) FREEZING OCCURRING.

FIGURE 31. - NEW PHYSICAL MODEL OF ICING PROCESS.

ORIGINAL PAGE IS
 OF POOR QUALITY

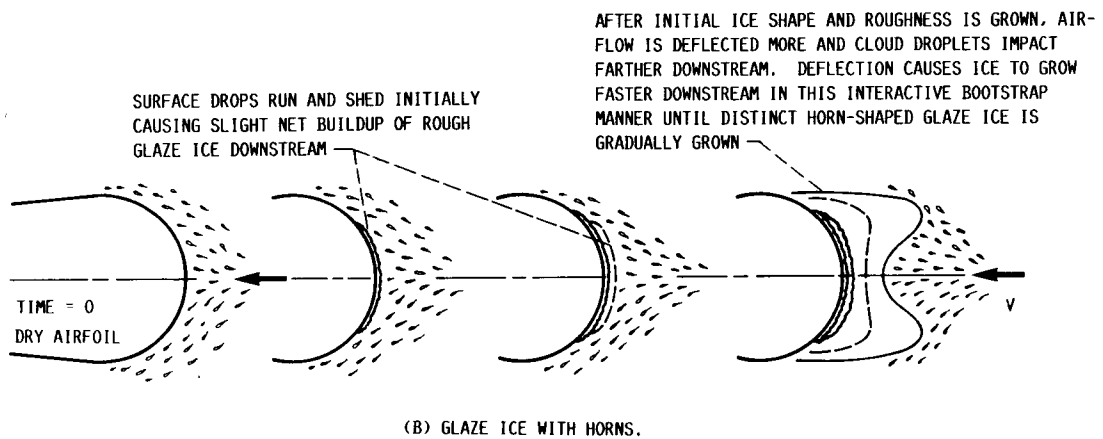
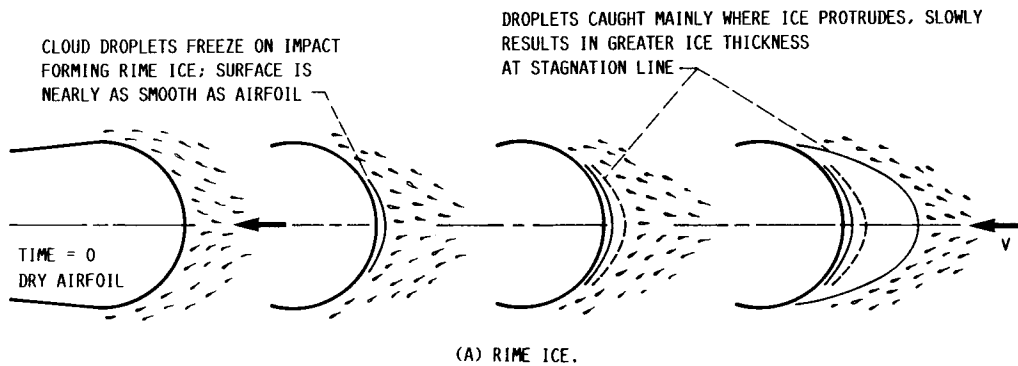


FIGURE 32. - GROWTH HISTORY OF RIME AND HORN-GLAZE ICE USING NEW PHYSICAL MODEL FOR ICING.



Report Documentation Page

| | | | | | |
|---|--|---|---|--|--------------------------|
| 1. Report No. NASA TM-87184 | | 2. Government Accession No. | | 3. Recipient's Catalog No. | |
| 4. Title and Subtitle Experimental Evidence for Modifying the Current Physical Model for Ice Accretion on Aircraft Surfaces | | | | 5. Report Date | |
| | | | | 6. Performing Organization Code | |
| 7. Author(s) W. Olsen and E. Walker | | | | 8. Performing Organization Report No. E-3658 | |
| | | | | 10. Work Unit No. 505-68-11 | |
| 9. Performing Organization Name and Address National Aeronautics and Space Administration Lewis Research Center Cleveland, Ohio 44135-3191 | | | | 11. Contract or Grant No. | |
| | | | | 13. Type of Report and Period Covered Technical Memorandum | |
| 12. Sponsoring Agency Name and Address National Aeronautics and Space Administration Washington, D.C. 20546-0001 | | | | 14. Sponsoring Agency Code | |
| | | | | | |
| 15. Supplementary Notes Prepared for the Third International Workshop on Atmospheric Icing of Structures, Vancouver, Canada, May 6-8, 1986. Film supplement to this report (Closeup Movies of Icing Over a Range of Airspeeds. NASA movie MPD-1683) can be obtained through the Photographic and Printing Branch, NASA Lewis Research Center, Cleveland, Ohio. | | | | | |
| 16. Abstract <p>Closeup movies were taken of the icing process at several positions along the surface of a small airfoil for a range of airspeeds (50 to 320 km/hr), air temperatures (above freezing down to -25 °C), and cloud conditions. These movies, still photographs (stop-action closeups), and other experimental data suggest that the current physical model for ice accretion needs significant modification at aircraft airspeeds. At aircraft airspeeds there was no flow of liquid over the surface of the ice after a short initial flow, even at subfreezing temperatures that are close to the freezing point. Instead there were very large stationary drops on the ice surface that lose water from their bottoms by freezing and replenish their liquid by catching the microscopic cloud droplets. This observation disagrees with the existing physical model for aircraft icing, which assumes there is a thin liquid film continuously flowing over the ice surface. This constant flow was thought to be the main cause of horn-shaped clear (glaze) ice. With no significant water flow over the ice surface, the freezing-fraction concept of the current physical model fails when a mass balance is performed on the surface water. Rime ice forms when the air temperature is low enough to cause the cloud droplets to freeze almost immediately on impact; that aspect of the existing model is correct. The movies and other results herein suggest the following changes to the current ice-accretion physical model. The characteristic shapes of horn-glaze ice or rime ice are primarily caused by the ice shape affecting the airflow locally and consequently the droplet catch and the resulting ice shape. In other words, ice that protrudes slightly will catch more droplets and, thereby, gradually grow faster than other nearby areas. Ice roughness plays a major role: it greatly increases the heat transfer coefficient, stops the movement of drops along the surface, and may also affect the airflow initially and, thereby, the droplet catch. At high subfreezing temperatures the initial flow and shedding of surface drops have a large effect on the ice shape; at the incipient freezing limit, no ice forms.</p> | | | | | |
| 17. Key Words (Suggested by Author(s)) Ice accretion physics | | | 18. Distribution Statement Unclassified - Unlimited Subject Category 03 | | |
| 19. Security Classif. (of this report) Unclassified | | 20. Security Classif. (of this page) Unclassified | | 21. No of pages 46 | 22. Price* A03 |